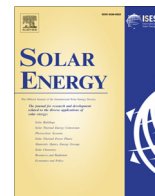




Contents lists available at ScienceDirect

Solar Energy

journal homepage: www.elsevier.com/locate/solener

Solar pyrolysis of carbonaceous feedstocks: A review

Kuo Zeng^{a,c}, Daniel Gauthier^a, José Soria^b, Germán Mazza^b, Gilles Flamant^{a,*}

^a Processes, Materials and Solar Energy Laboratory, PROMES-CNRS, 7 rue du Four Solaire, 66120 Font Romeu, France

^b Institute for Research and Development in Process Engineering, Biotechnology and Alternative Energies (PROBIEN, CONICET – UNCo), 1400 Buenos Aires St., 8300 Neuquén, Argentina

^c State Key Laboratory of Coal Combustion, School of Energy and Power Engineering, Huazhong University of Science and Technology, Wuhan 430074, China

ARTICLE INFO

Article history:

Received 13 March 2017

Received in revised form 5 May 2017

Accepted 9 May 2017

Available online xxxxx

Keywords:

Solar energy

Pyrolysis

Carbonaceous feedstock

Solar fuels

ABSTRACT

Solar pyrolysis of a carbonaceous feedstock (coal, biomass and wastes) is a process in which carbon-containing feedstocks are used as chemical reactants and solar energy is supplied as high-temperature process heat. This process has the potential to produce higher calorific value products with lower CO₂ emissions than conventional pyrolysis processes. As a consequence, the intermittent solar energy is chemically stored in the form of solar fuels. Solar pyrolysis was first demonstrated in an indoor environment using a solar simulator (image furnace) for exploring the fundamental mechanisms of carbonaceous feedstock pyrolysis under severe radiative conditions (high temperatures and heating rates) in comparison to conventional pyrolysis. More recently, low-temperature solar pyrolysis has been demonstrated to be a good technology for bio-oil production. Our high-temperature solar pyrolysis process produces more combustible gas products than other processes. This paper reviews developments in the field of solar pyrolysis processing by considering fundamental mechanisms, experimental demonstrations, models and challenges.

© 2017 Elsevier Ltd. All rights reserved.

1. Introduction

Fossil fuels supply approximately 78.4% of the world's overall energy needs in 2013 which are widely used for transportation, electricity generation, industrial processes, and heating. At the same time, fossil fuel combustion is a major source of greenhouse gas emissions, which are contributing to global warming. Moreover, there is an increasing awareness that the increased deployment of renewable energy, such as solar energy, is critical for addressing climate change, the energy crisis and creating new economic opportunities. In 2013, renewable energy contributed 19% of the global energy consumption. Of the renewable energy sources, solar energy contributed less than 1.0%, as shown in Fig. 1 (REN21, 2014). Fig. 2 indicates that the expected development of renewable energy production between 2010 and 2040 (from 19% to 47.7%) will include a significant increase in solar energy (from 0.24% to 10%) (IEA, 2014).

Solar energy is viewed by some experts as the alternative with the greatest intermediate to long-term potential to replace fossil fuels. Solar energy technology development has been largely focused on electricity generation. While solar energy is important, solar electricity does not fulfill the main advantages of high-energy

density fuels (accounting for approximately 70% of the overall energy needs) for transportation, industrial processes, and heating. Consequently, it is important to utilize solar energy for the production of clean alternative fuels (Bensaid et al., 2012). Two important challenges must be overcome to attain this goal. The first challenge is the need to increase the solar radiation flux density given the dilution of terrestrial solar radiation (only approximately 1 kW/m² for a clear day). Optical reflective concentration devices (such as parabolic troughs, linear Fresnel reflectors, parabolic dishes and central towers) have been used to focus incident solar radiation on surfaces that are much smaller than the collection surfaces of the mirrors. The second challenge is the need to provide appropriate reactants for the conversion of intermittent solar energy into fuels. Carbonaceous feedstocks (coal, biomass and wastes) consisting of carbon and hydrogen could be appropriate reactants because they can store energy in the combustible form due to thermochemical transformation. There are two solar thermochemical processes that combine concentrated solar energy and carbonaceous feedstocks together for converting solar energy to chemical fuels. The first process is solar gasification for syngas production, which has been investigated in the last 20 years (Piatkowski et al., 2011). The second process is solar pyrolysis for bio-oil, biochar and gas production, which entered the research field in the last 40 years and now has garnered renewed interest (Zeng et al., 2015a,

* Corresponding author.

E-mail address: gilles.flamant@promes.cnrs.fr (G. Flamant).

Nomenclature

Latin letters

A	pre-exponential factor (1/s)
a	stoichiometric coefficient for gas (-)
b	stoichiometric coefficient for tar (-)
C_p	heat capacity (J/kg/K)
D	diffusion coefficient (m^2/s)
E	activation energy (J/mol)
F	momentum source term (Pa/m)
g	gravity (m/s^2)
k	reaction rate constant (1/s)
L	length (m)
M	molar mass/moisture content (kg/mol/wt%)
m	mass (kg)
P	pressure (Pa)
Q	heat generation (W/m^3)
R	radius (m)
R_g	ideal gas constant (J/mol/K)
x	cylindrical coordinate m
r	cylindrical coordinate m
S	source term ($kg/m^3/s$)
T	temperature (K)
t	time (s)
v	velocity (m/s)
HHV	higher heating value (MJ/kg)
LHV	lower heating value (MJ/kg)
X	mass fraction (wt%)
U	upgrade factor (-)
\bar{u}	intrinsic velocity vector (m/s)

Greek letters

Δh	reaction heat (J/kg)
ΔT	temperature difference (K)
Δt	time difference (s)

ε/ξ	porosity (-)
$\lambda/\bar{\lambda}$	thermal conductivity (W/m/K)
μ	viscosity (Pa s)
ρ	apparent density (kg/m^3)
η	pyrolysis degree/Efficiency (-)
ω	reaction term ($kg/m^3/s$)

Subscripts

s	solid
i	component (w, c, is)
Ar	argon
c	char
cond	conductive
eff	effective
g	gas
is	intermediate solid
r	radial direction
rad	radiative
t1	primary tar
t2	secondary tar
V	volatiles (g, t1, t2)
w	wood
C	carbon
H	hydrogen
O	oxygen
N	nitrogen
S	sulfur
A	ash
oil	bio-oil product
gas	gas product
char	biochar product
feedstock	carbonaceous feedstock

2015b, 2015c, 2016, 2017a, 2017b, 2014, 2015; Li et al., 2016; Soria et al., 2017).

Gasification is a process in which carbonaceous materials are reacted with a controlled amount of oxygen, CO_2 and/or steam at high temperatures ($>700\text{ }^\circ\text{C}$) to produce CO , H_2 and CO_2 . However, the generation of unwanted char and tar is a serious issue preventing the broad implementation of gasification technology. In contrast, if the carbonaceous feedstock is heated in the absence

of oxygen, then a mixture of gases, bio-oils, and biochars is generated. The most obvious differences between solar gasification and solar pyrolysis are the different reaction pathways caused by the differences in the surrounding atmosphere. Solar gasification itself combines solar pyrolysis and subsequent oxidation reactions. During the solar pyrolysis process, the concentrated solar radiation supplies high-temperature process heat for carbonaceous feedstock pyrolysis reactions (Chueh et al., 2010). Then, solar energy

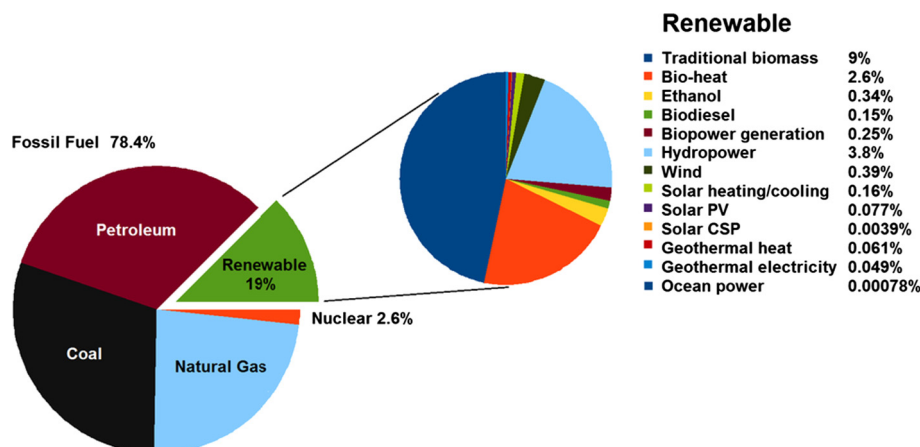


Fig. 1. Total world energy consumption by source in 2013 (REN21, 2014).

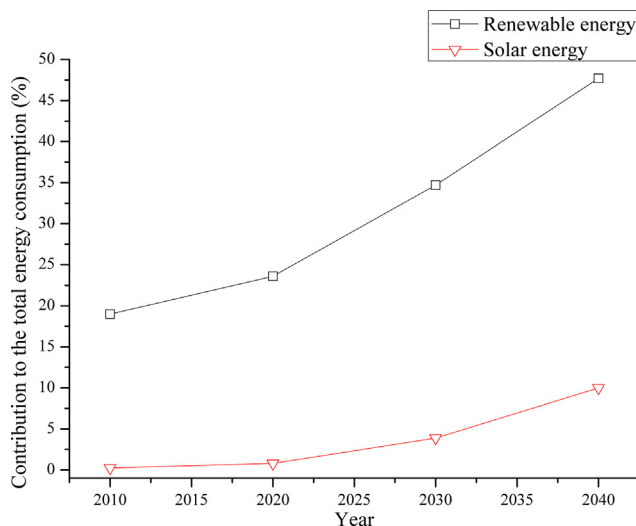


Fig. 2. Global renewable energy scenario between 2010 and 2040 (IEA, 2014).

is converted into transportable and dispatchable solar fuels (bio-oils, biochars and gases) (Zeng et al., 2015b). Bio-oil can be used as a combustion fuel for transport or electricity and heat production or as a feedstock for the production of chemicals (Czernik and Bridgwater, 2004). Biochar is attractive as a substitute fuel or for the filtration and adsorption of pollutants (Kan et al., 2016). The gas products have various potential applications, such as being directly used for heat or electricity production, producing individual gas components (CH_4 , H_2), or synthesizing liquid bio-fuels (Hossain and Davies, 2013).

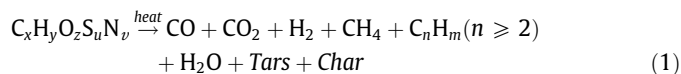
Compared with conventional autothermal pyrolysis, some advantages of solar pyrolysis are as follows: (1) Solar fired pyrolysis systems are capable of faster startup and shutdown (Hofmann and Antal, 1984). (2) In conventional pyrolysis, a portion of the raw materials is burned to generate the process heat required for pyrolysis. This reduces the amount of feedstock available for pyrolysis and pollutes the produced gases with combustion gases. In contrast, the heat required for solar pyrolysis is supplied by concentrated solar radiation, which valorizes all of the feedstocks as useful products. Hence, using solar energy maximizes the amount of products and reduces pollution at the same time (Romero and Steinfeld, 2012). (3) The carbonaceous feedstock energy content is upgraded because the solar energy provides a pyrolysis reaction enthalpy that is transferred to the products, which is a suitable method for storing intermittent solar energy in the form of chemical energy (Kodama, 2003; Nzihou et al., 2012; Yadav and Banerjee, 2016). For example, the minimum energy gained by a solar pyrolysis process may be estimated based on an enthalpy balance that accounts for the mass of feedstock that is burned to provide the heat of reaction during a conventional autothermal pyrolysis. Consequently, at least the same proportion of solar energy is stored in the products if the feedstock is processed using solar high-temperature heat. (4) The volatiles evolved from pyrolysis experience a low-temperature zone just after they are produced at the sample surface in direct irradiation solar reactors once they pass the focus of the solar furnace (Hopkins et al., 1984). The volatiles passing from the hot zone (heated by the sunbeam) to the cool zone (the surrounding gas) are quickly quenched, minimizing the secondary reactions that convert tar into gas. Hence, the two-temperature effect in a direct irradiation solar reactor can be considered to be advantageous for producing useful bio-oils at common pyrolysis temperatures of approximately 500 °C. (5) Conversely, highly concentrated solar radiation can directly reach the raw material surface within a very short time.

Therefore, solar pyrolysis has the advantages of high temperatures and fast heating rates (Lédé, 1999). Consequently, under these conditions, the solar pyrolysis tends to generate more gas at high pyrolysis temperatures of approximately 1200 °C (Zeng et al., 2015b, 2015c, 2016, 2017a).

This paper discusses the solar pyrolysis of carbonaceous feedstocks for converting solar energy into solar fuels. Concentrated solar energy acts as the process heat source to drive the pyrolysis reaction of carbonaceous feedstocks (coal, biomass and wastes) to generate solar fuels. The fuels that are sustainably produced in liquid, solid and gaseous form (bio-oil, biochar and gas, respectively) offer multiple benefits in terms of their energy security, compatibility with existing infrastructure, and climate change mitigation. In the first part of this review, we describe the fundamental principles of carbonaceous feedstock pyrolysis. In the secondary part, we demonstrate how concentrated solar energy is integrated into the carbonaceous feedstock pyrolysis process. First, solar simulators (image furnaces) have been used for exploring the fundamental mechanisms of carbonaceous feedstock pyrolysis. Then, from the application point of view, two kinds of target products have been obtained from solar furnaces: (1) bio-oils at low temperatures (around 500 °C) and (2) gases at high temperatures (around 1200 °C). The experimental energy upgrade factors of classical and solar pyrolysis are compared. Furthermore, a summary of solar pyrolysis prototypes is included. In the third part, examples of modeling work are analyzed for interpreting the experimental results and designing solar reactors. Finally, we identify the critical challenges and key issues for the future large-scale development of solar pyrolysis processes.

2. Principles of carbonaceous feedstock pyrolysis

Carbonaceous feedstock pyrolysis is the thermal decomposition of raw materials in the absence of oxygen into gaseous products (mainly CO_2 , CO , H_2 , CH_4 , C_2H_2 , C_2H_4 , C_2H_6 , etc.), liquid products (tar, high-molecular-weight hydrocarbons and water) and solid products (char). The theoretical pyrolysis reaction can be represented as (Piatkowski et al., 2011):



The three steps of carbonaceous feedstock pyrolysis processes are illustrated in Fig. 3 (Neves et al., 2011). The sample is first dried with a slight weight loss between 100 °C and 200 °C. Some internal rearrangements, such as bond breakages, occur with free radical and carbonyl group formation. At the same time, a small release of water, carbon monoxide and carbon dioxide occurs. The primary pyrolysis stage occurs at 250 °C and ends at approximately 500 °C, producing the primary products (denoted by “1” in Fig. 3). Solid decomposition occurs with significant weight loss during the primary pyrolysis. The primary products can further participate in various secondary reactions when the sample is heated at higher temperatures, forming the final products (denoted by “2” in Fig. 3). There are three stages during the primary vapor secondary reactions, as shown in Fig. 4 (Evans and Milne, 1987). Between 500 and 600 °C, the higher molecular weight products slightly break into lighter aromatics and oxygenate in less than one second. The secondary stage, approximately 700 °C, is the formation of CO , light olefins, and aromatics (from carbohydrates). At higher temperatures, the third stage leads to tertiary product (polynuclear aromatics) formation.

The pyrolysis product distribution depends on the pyrolysis method, the characteristics of the carbonaceous feedstock and the reaction parameters. Table 1 summarizes the main biomass pyrolysis technologies and their major products (Liu et al.,

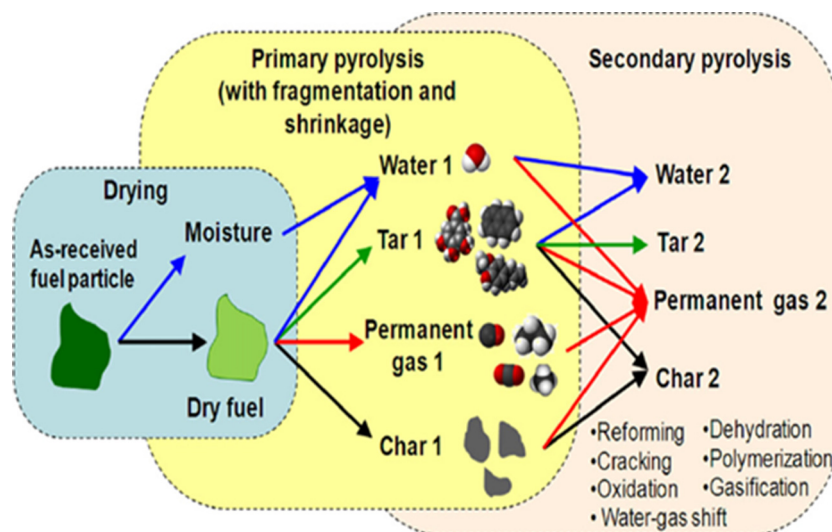


Fig. 3. Pyrolysis of wet carbonaceous feedstocks: drying, primary pyrolysis and secondary pyrolysis. The arrows indicate the main routes for product formation (from Neves et al. (2011)).

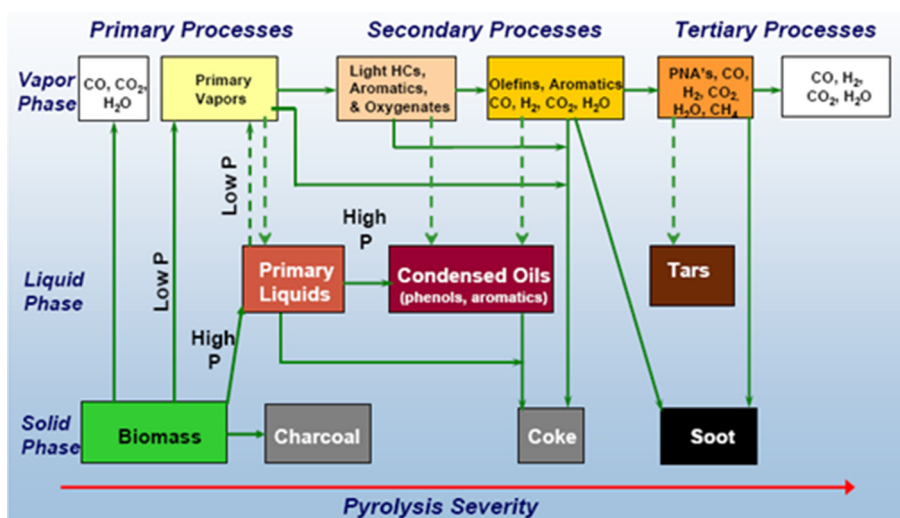


Fig. 4. Carbonaceous feedstock pyrolysis pathways (from Evans and Milne (1987)).

Table 1
Pyrolysis technology, processing conditions and product distributions (from Liu et al. (2014)).

Pyrolysis technology	Process conditions			Product yields		
	Residence time	Heating rate	Temperature (°C)	Liquid (wt%)	Solid (wt%)	Gas (wt%)
Slow	5–30 min	<50 °C/min	400–600	<30	<35	<40
Fast	5 s<	10–200 °C/s	400–600	<75	<25	<20
Flash	0.1 sM<	~1000 °C/s	650–900	<20%	<20%	<70%

2014). Charcoal production involves mainly slow pyrolysis at low temperatures and low heating rates (Antal et al., 1990). During slow pyrolysis, the vapor residence time is high (5–30 min), and the vapor phase components continue to react with each other, resulting in the formation of solid char and other liquids (Bridgwater et al., 2001). Fast pyrolysis processes are receiving increased attention for producing liquid products (Pütün, 2002). The basic characteristics of fast pyrolysis processes include high heat transfer and heating rates, very short vapor residence times, rapid vapor cooling and precision control of the reaction temperature (approximately 500 °C) (Demibas and

Arin, 2002). Fast pyrolysis processes produce 60–75 wt% liquid bio-oils, 15–25 wt% of solid chars and 10–20 wt% noncondensable gases, depending on the feedstock used (Mohan et al., 2006). Flash pyrolysis is sometimes considered to be a very fast pyrolysis process (Demibas and Arin, 2002), usually in the context of laboratory studies involving the rapid movement of a small particle through a drop tube or under gas flow. Higher temperatures and shorter residence times than fast pyrolysis are also used. At higher temperatures, primary vapor secondary reactions are more likely to happen, which leads to higher gas production (up to 75%) than in flash pyrolysis.

3. Pyrolysis in solar simulators and solar furnaces

In a research study, solar pyrolysis was first demonstrated in an indoor environment using a solar simulator (image furnace) that associated high-power lamps with specific mirrors. Since then, solar pyrolysis experiments have been conducted under various conditions (different types of carbonaceous feedstocks, heating parameters and reactors). Multiple results have provided new insights into the fundamental mechanisms of solar pyrolysis with carbonaceous feedstocks. More recently, carbonaceous feedstock pyrolysis has been tested in a solar furnace (SF) with real solar input. Different heating parameters were tested for optimizing the production of targeted products (bio-oils or gases).

3.1. Solar pyrolysis with a solar simulator

3.1.1. Solar simulator principle

Image furnaces (solar simulators) are used for studying chemical reactions in radiative heating conditions. Concentrating mirrors or lenses focus the light from a high-power discharge lamp onto a solid surface (the sample). Image furnaces were first developed using carbon arcs as the light source and elliptic or parabolic mirrors as the concentrator in the 1950s (Glaser and Walker, 1962). In the 1960s, xenon and mercury-xenon arc lamps were implemented as a more powerful source. In the 1980s, some pioneering works using image furnaces for biomass pyrolysis were reported (Hopkins et al., 1984; L  d   et al., 1987; Caubet et al., 1982; Chan et al., 1985; Antal et al., 1983; Tabatabaie-Raissi and Antal, 1986). In the 1990s and 2000s, other pyrolysis fundamental studies that applied image furnaces were published (Gr  nli and Melaaen, 2000; Gr  nli, 1996; Boutin et al., 2002). In the 2010s, some image furnaces were used to simulate solid high-temperature thermochemical reactions in conventional reactors (Authier and L  d  , 2013; Christodoulou et al., 2013). Compared to other traditional furnaces used for pyrolysis, image furnaces (solar simulators) have some advantages and drawbacks, as listed in Table 2 (Authier and L  d  , 2013).

3.1.2. Small particle pyrolysis with a solar simulator

Antal et al. (1980) first simulated the biomass solar pyrolysis process with high-power tungsten halogen bulbs connected to two elliptical mirrors. The horizontal and vertical beam systems were tested with the reactor set in the axis of the elliptical mirror.

Table 2

The advantages and drawbacks of image furnaces (adapted from Authier and L  d   (2013)).

Advantages	Drawbacks
The feedstock is directly heated by concentrated radiation. The sweeping gas and reactor remain relatively "cold", which can prevent secondary reactions of the primary pyrolysis products	Because the optical properties of the feedstock change during the pyrolysis reaction, it is very difficult to determine the actual absorbed heat flux density and temperature on the sample surface
The heat flux density corresponding to the temperature at the feedstock surface can be measured and adjusted using shutters	Some reaction byproducts, such as tar, may deposit on the reactor wall, reducing the incident radiation
The concentrated radiation can be focused on a predefined location at a desired time	The feedstock may shrink under long heating times, and the surface may move out of the image furnace focus
The heating conditions are very clean without combustion	Their focal zone cross section is very small. They cannot be operated with a big size sample
They can simulate large-scale solar furnaces at the laboratory scale	

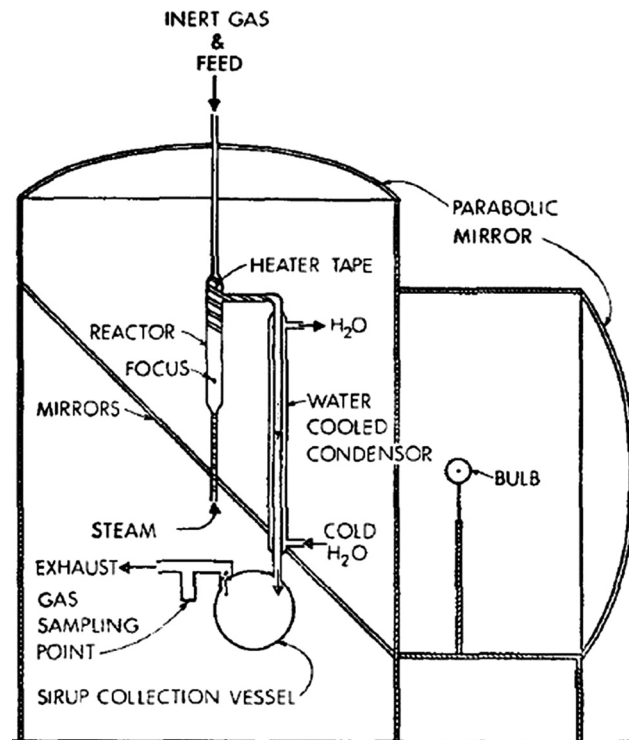


Fig. 5. Arc image furnace (from Hopkins et al. (1984)).

High liquid (syrup) yields (up to 70%) were obtained due to the absence of gas-phase reactions at very low gas temperatures and short residence times. The solar pyrolysis reactor decoupled the gas reaction from the solid reaction, which could be used to isolate the liquid (syrup) or gas products. However, it was impossible to reach complete pyrolysis (50% maximum) because all the particles did not cross the furnace focus. Encouraged by the first solar pyrolysis results, Hopkins et al. (1984) used a spouted-bed reactor and an arc image furnace to prepare high syrup yields by taking advantage of the quench effects (two temperature reactors) produced during radiant flash pyrolysis. The spouted-bed reactor was composed of a 22 mm inner diameter quartz tube with a wall thickness of 1.5 mm. It had a tapered conical bottom with a cone angle of 20°. A 1 mm capillary tube that was collinear to the reactor axis was located at the base of the cone. The image furnace consisted of a 5 kW short-arc Xenon bulb as the energy source and a concentrating system. The latter was composed of a set of twenty-four 30 × 38 cm flat glass mirrors and two 1.5 m diameter parabolic mirrors (Fig. 5). The total power delivered to the focal zone was 150 W. A flux density that reached 2 MW/m² was obtained at the focus. Then, 2–8 g of biomass particles were fed into the top of the reactor using a vibrating feeder. Steam entered the reactor through a capillary tube for spouting the bed. The mix zone was adjusted at the image furnace focus, causing the particles to be repeatedly heated when they passed through the focus. The pyrolysis process produced 63% and 30% syrups from cellulose and Kraft paper, respectively. The high syrup yields were due to the quench effects (two temperature reactors). The syrup was quickly removed from the hot temperature zone (focus) before it could decompose.

Hopkins et al. (1984) pyrolyzed biomass (a few tens of milligrams) in a vacuum using a xenon flashtube to study the primary mechanisms of biomass pyrolysis in more detail. The biomass feedstock was placed inside a sealed tubular Pyrex reactor, which was then evacuated and inserted into a helical xenon flashtube core. The lamp was surrounded by a polished cylindrical aluminum reflector, which increased the light intensity. The lamp was

oriented so that its helical axis was horizontal and was powered by the energy release of a 200- μ F capacitor bank. The capacitors could be charged to a maximum of 100 kV; thus, the maximum total energy available for the flash was 10 kJ. The flux density exceeded 80 MW/m² during the 1 ms flash. The syrup yields were low (average 25%), while the gas yields were comparatively high (average 32%). The gaseous products were composed primarily of CO, C₂H₂ and H₂, with CO/CO₂ mass ratios ranging between 8 and 20; these values were higher than those observed during low-temperature pyrolysis (less than 1). The high relative yields of CO were attributed to a high-temperature solid-phase pyrolysis pathway involving catastrophic fragmentation of the polymer structure during flash pyrolysis of the biomass materials.

A bench-scale solar simulator was designed and fabricated at the University of Hawaii (Tabatabaie-Raissi and Antal, 1986). The light source was a 30 kW water-cooled short-arc high-pressure xenon lamp. The optics of the solar simulator included two 1.52 m diameter parabolic dish reflectors with 0.648 m focal lengths. The solar simulator provided concentrated radiation with a total thermal power of 2 kW and a maximum flux density of 10 MW/m². Based on the built-up bench-scale solar simulator, the researchers designed a fast thermo-gravimetric analyzer (TGA) to determine the kinetics of cellulose pyrolysis in a simulated solar environment (Tabatabaie-Raissi et al., 1989). First, 5–10 mg of cellulose powder was placed inside a small metallic holder shielded by a small platinum lid. A very thin thermocouple was located inside the sample holder. This assembly was placed in a fused silica tube and filled with N₂ flow. The decomposition of Avicel PH105 microcrystalline cellulose under the conditions of high heating rates (greater than 2 K/s) and high temperatures was modeled using a simple single-step (nearly) first-order reaction with an overall rate coefficient of $k = (1.2 \pm 0.6) \times 10^6 \exp [-(100.5 \pm 3)/RT] \text{ s}^{-1}$, which was in good agreement with the rate

constants reported from the low-temperature studies. The char constituted a substantial portion of the remaining residue after pyrolysis and accounted for more than 8 wt% of the original dry material.

According to carbonaceous feedstock pyrolysis pathways, intermediate vapor phase compounds exist before quenching occurs. High-energy photons from concentrated sunlight can photodissociate certain vapor phase compounds, producing free radicals. The pyrolysis reactions involving hydrocarbons can be initiated or influenced by these free radicals. Hunjan et al. (1989) conducted experiments using a new horizontal-axis image furnace for determining the photocatalytic formation of free radicals and their effects on hydrocarbon pyrolysis chemistry. The experimental apparatus consisted of two major subsystems: a 1-kW arc image furnace and a fused silica vapor-phase tubular flow reactor. The light emitted from the xenon arc lamp between 200 and 2000 nm was used to photo-dissociate the acetone. For the free radical formation experiments, a mixture of Fisher Scientific HPLC grade acetone (99.5% purity) and steam was injected into the reactor at 150 °C. For the pyrolysis experiments, acetone was introduced with n-butane at 350 °C. The acetone was readily photodissociated in a 1000 sun environment, yielding methyl radicals. Methyl radicals sensitized the pyrolysis chemistry of n-butane at temperatures as low as 350 °C. These methyl radicals enhanced the n-butane cracking, leading to the formation of lighter alkanes and alkenes. Without photosensitization, no pyrolysis occurred. Photosensitization of the hydrocarbon cracking reactions could be enhanced between 400 and 500 °C due to the increased chain lengths at higher temperatures.

3.1.3. Large particle pyrolysis with a solar simulator

Large particle wood pellets with thicknesses ranging from 5 to 15 mm have been pyrolyzed in a single-particle glass reactor

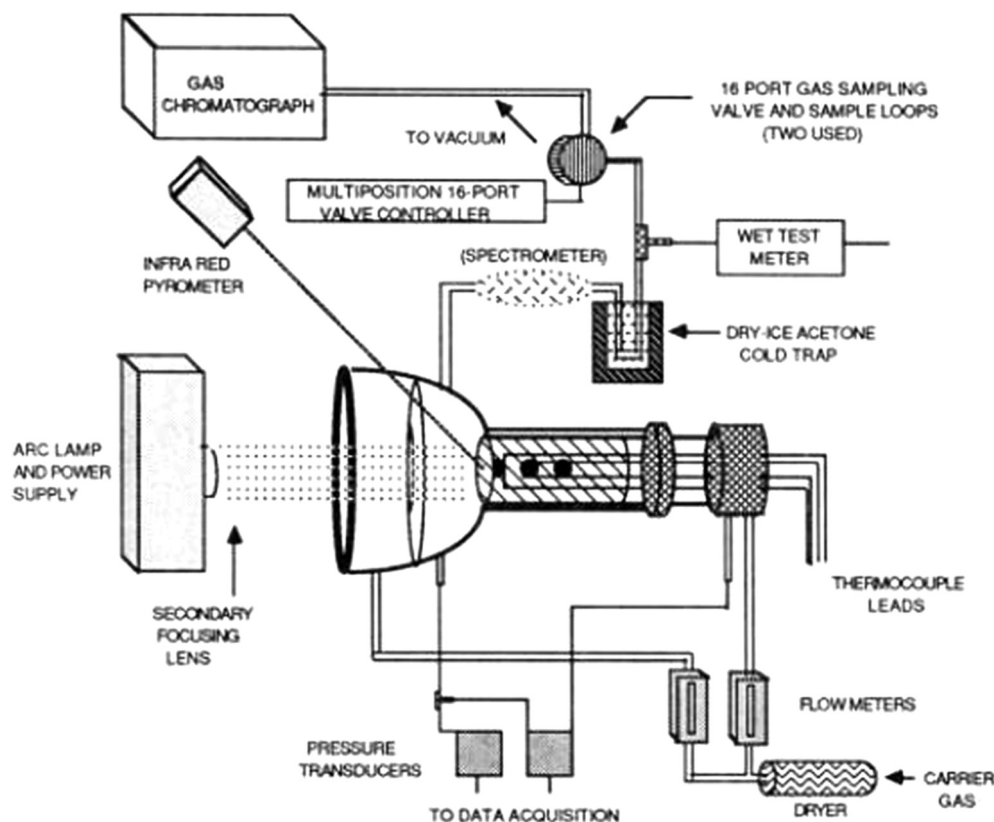


Fig. 6. Single-particle reactor and analysis system (from Chan et al. (1988)).

Table 3

Mean values and standard deviations (\pm) of the converted fraction, axial shrinkage, and ultimate product yield distributions obtained from the pyrolysis of spruce (Grønli and Melaen, 2000; Grønli, 1996).

	Low heat flux (80 kW/m ²)		High heat flux (130 kW/m ²)
	5 min heating	10 min heating	10 min heating
Converted fraction (wt%)	25.7 \pm 1.63	45.5 \pm 3.61	72.1 \pm 3.05
Axial shrinkage (%)	2.9 \pm 0.75	2.7 \pm 2.34	1.5 \pm 0.92
Char yield (wt%)	26.2 \pm 0.53	28.7 \pm 1.06	27.0 \pm 0.06
Tar yield (wt%)	38.0 \pm 1.22	31.3 \pm 5.06	27.9 \pm 0.61
Gas yield (wt%)	35.9 \pm 1.44	40.0 \pm 5.45	45.2 \pm 0.62

shown in Fig. 6 (Chan et al., 1985, 1988). It contained wood samples in a sleeve and tube. The incident radiation passed through a large-diameter window. The ports and baffle eliminated volatiles condensation on the window and decreased the gas residence time in the reactor. The whole system included a 1000-W xenon arc lamp that provided one-dimensional heating (horizontal direction) with an absolute flux density from 0 to 250 kW/m² (Chan et al., 1985, 1988). The temperature was monitored using fine chromel-alumel thermocouples inserted 2 and 4 mm from the irradiated surface and 6 mm from the surface if the particles were sufficiently thick. The surface temperature was measured with a calibrated infrared pyrometer. The sides of the sample were insulated by two Pyrex glass tubing layers. Helium carrier gas rapidly quenched the outflowing volatiles and swept products toward the traps and the analysis system. The water release rate was measured as a function of time using an infrared spectrometer. For all experiments, the reaction products that condensed in the cold trap were defined as tar. Uncondensed gases were sampled from the cold trap exit using programmable, calibrated volume-sampling valves. Immediately after the experiment, the gases were analyzed using gas chromatography (GC). There was a combined effect between the particle thickness and the heat flux on the pyrolysis product distribution. The secondary tar reactions were enhanced at high temperatures and extended residence times inside the particle. Thus, the lowest tar yield, corresponding to the highest gas yield, was obtained by applying the highest heat fluxes to the thickest particles.

One face of a uniform cylinder ($D = 20$ mm, $L = 30$ mm) was one-dimensionally heated in a single-particle bell-shaped Pyrex reactor using a xenon arc lamp in a study on wood (Norwegian birch, pine and spruce) pellet pyrolysis (Grønli and Melaen, 2000; Grønli, 1996). The xenon arc lamp provided a high radiant heat flux. The front face of the reactor consisted of a fused silica window that enabled the maximum transmission of radiant energy (with approximately a 10% loss). The reactor had three inlet ports for the purge gas (N_2) located close to the window to keep the hood free from smoke and to prevent volatiles condensation on the window. Two different heat fluxes, 80 kW/m² (low heat flux) and 130 kW/m² (high heat flux), were used. The surface and in-depth temperatures were significantly higher when exposed to a higher heat flux. A noticeable temperature plateau of approximately 380 °C was observed due to the rapid decrease in the local thermal conductivity when the substrate transformed from wood into a more porous char. The measured mean values and standard deviations of the converted fraction, axial shrinkage, and ultimate product yield distributions (char, tar, and gas yields) are presented in Table 3. When the heating time increased from 5 to 10 min, the converted fraction increased by almost 77%; the ultimate yields of the char and noncondensable gases also increased, while the yield of the condensable species (tar/water) decreased. By increasing the heat flux from 80 to 130 kW/m², the converted fraction

increased by almost 59%, and the ultimate yields of the char and condensable species (tar/water) decreased, while the yield of the noncondensable gases increased. The char layer thickness increased as a consequence of a longer pyrolysis time or higher heat flux. Hence, the residence time of the pyrolysis species in the hot char layer increased, which promoting secondary reactions of the heavy tar into gas.

3.1.4. Studies on primary pyrolysis reaction with a solar simulator

The research group of Lédé utilized a solar simulator to explore the uncertainties and controversies of carbonaceous feedstock pyrolysis (Lédé, 1999). The concentrated radiation provided high heat flux densities (higher than 1 MW/m²) in very clean conditions. The feedstock was irradiated for short durations, less than 1 s, to prevent secondary reactions. The nature of primary pyrolysis was elucidated by observing and analyzing the feedstock surface. It was also possible to measure some of the optical properties of the intermediates.

First, the horizontal setup was used for small cellulose particle (450 ± 50 μ m thickness) pyrolysis (Boutin et al., 2002). Fig. 7 illustrates the experimental setup. The light source was an air-cooled 5 kW xenon high-pressure lamp. The cross section of the concentrated light was focused inside an approximately 5 mm diameter circle. The mean available flux densities varied between 1 and 7.4 MW/m² by setting the diaphragms at different locations between F2 and F2. The flash time was adjusted by using of a controlled pendulum that intercepted the incident light. A photocell facing the second mirror and connected to a computer made the flash duration as short as 0.01 s. The experiments revealed the presence of short lifetime intermediate liquid compound (ILC) species formed during the flash pyrolysis of cellulose. The short lifetime products were liquid at the reaction temperature but solid at room temperature. They were soluble in water and produced vapors in the gas phase without char formation for heating times longer than 1 s.

A horizontal image furnace with only a second elliptical mirror was used for massive-sample pyrolysis (Boutin et al., 2002; Lédé et al., 2002). The reactor was a transparent quartz cylinder (inside diameter = 3 cm, height = 5 cm) with conical parts at its bottom and top. The cellulose pellets, 5 mm in diameter and a few millimeters high, were held at their center and adjusted to the furnace focus with three micrometric screws. The cellulose mass loss and the produced vapor and gas increased linearly with the heating time. The ILCs decomposed into condensable vapors and gases as well as chars under the low flux density. The variation of the CO, H₂ and hydrocarbon masses as a function of the heating time (between 0.05 and several seconds) were almost linear. The hydrocarbons contributed to almost 50% of all the gases produced under the high heat flux, which strongly decreased to approximately 20% under the low heat flux. The gas species were produced after approximately 0.12–0.16 s under the high heat flux (4 MW/m²) and 2.1–2.6 s under the low heat flux (0.46 MW/m²). The molar fraction of CO/H₂ varied between 1.6 and 3 in all cases.

After characterizing the cellulose pyrolysis after heating with concentrated solar radiation, flash pyrolysis of a lignin sample with an image furnace was also carried out to produce hydrogen (Baumlin et al., 2006). Fast pyrolysis using Kraft lignin (KL) pellets (10 mm in diameter and a few millimeters in height) was performed under a 7.4 MW/m² radiant flux density. All the masses varied linearly with the heating time between 0.05 and 3 s. The lignin mass loss, char and gas formation occurred almost simultaneously, faster than for cellulose. High molar fractions of H₂ (approximately 50%) were obtained, which did not vary with the heating time. The CO mole fraction increased with the flash time from 33% to 44%, while the CO₂ decreased from 12% to 2%. The light hydrocarbon (mainly CH₄ with minor fractions of C₂H₂, C₂H₄, C₂H₆

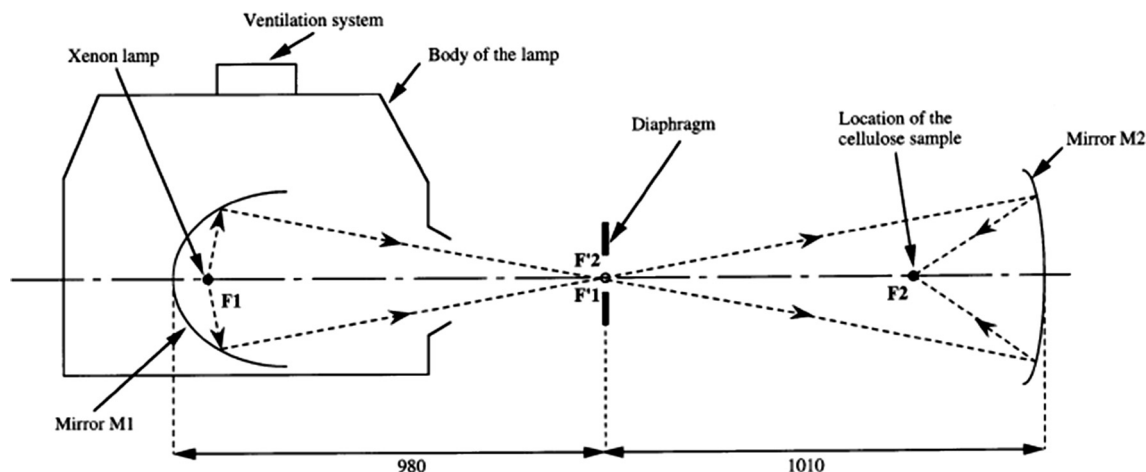


Fig. 7. Horizontal image furnace (size in mm) (from Boutin et al. (1998)).

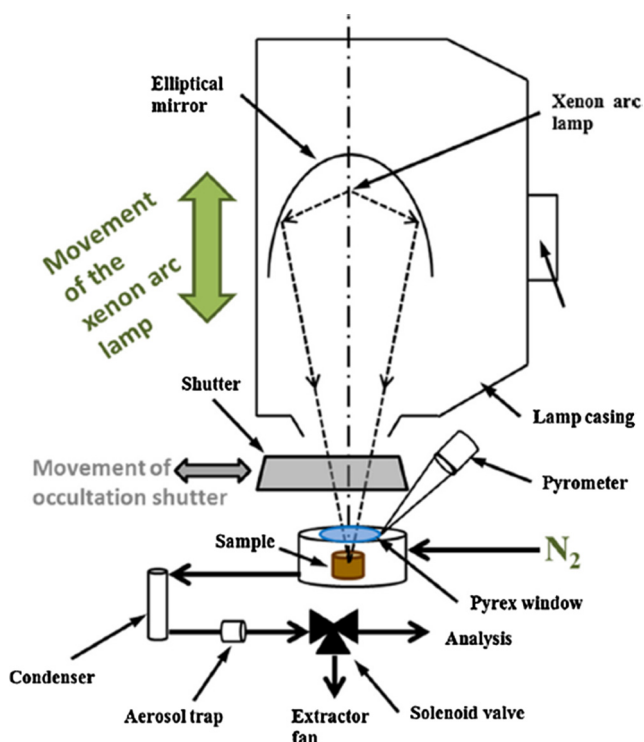


Fig. 8. Vertical image furnace (from Christodoulou et al. (2013)).

and C_3H_8) mole fractions were always very low, between 1% and 6%. The masses of H_2 and CO increased linearly as a function of the flash time for $t_f < 3$ s.

In addition, a vertical-axis image furnace has been developed (Fig. 8) (Christodoulou et al., 2013). A 5 kW xenon high-pressure arc lamp was set at the first focus of an elliptical mirror. The sample was placed at the second focus, where the light was concentrated. The heat flux density applied to the sample as a function of time was adjusted by moving the lamp. The lamp movement system was controlled by a computer with the initial position, final position and motion speed as the control parameters. A power sensor measured the heat flux density according to the lamp position. An occultation shutter controlled the flash with an accuracy of 10 ms. The reactor was composed of two parts. The first part was a stainless steel cylinder (5.5 cm inside diameter and 5 cm high)

with a Pyrex window (3.5 cm diameter and 3.3 mm high) on its top. The second part contained an air cooling jacket for the pyrometer, which was also swept with nitrogen.

Most fundamental pyrolysis studies have focused on the effect of the flash time (heating time) on the product variations. The influence of the heat flux density on the product yield, gas composition and reaction rate of wood pyrolysis has also been investigated using an image furnace, as shown in Table 4 (Authier and Lédé, 2013; Authier et al., 2009). The mass balance is about 92% mainly due to missing condensable vapor. Condensable vapor yields comprised the majority (approximately 60%) of the products and did not significantly change with the heat flux density. The gas yield increased by approximately 10 times when the heat flux density increased by a factor of 10. At the same time, the char fraction decreased, confirming that the process increasingly approached slow pyrolysis conditions as the heat flux density decreased.

3.2. Low temperature pyrolysis with a solar furnace for bio-oil production

Antal et al. (1983) designed and operated a solar fired biomass flash pyrolysis reactor for syrup production. The maximum flux density in the focal zone was on the order of 1.25 MW/m^2 , which corresponded to the maximum total power of 400 kW. First, 3–255 g/min of biomass particles with diameter between 425 and 710 μm (cellulose, corn cob and hardwood) were fed at the top of a vertical quartz tube reactor with screw feeder. The biomass fell into a region of intense solar radiation that was surrounded by a water-cooled reflective cylindrical cavity. Then, 200–1000 ml/min of nitrogen was used to purge the screw feeder and remove the gas phase pyrolysis products (vapors and gases). The char was collected at the bottom of the reactor with a char bucket. The vapors and gases were trapped at the top of the reactor for further analysis. A maximum of 50% of the biomass particles were pyrolyzed due to an insufficient residence time in the hot temperature focus zone. Then, steam flowed upward to create a countercurrent flow of biomass particles and gases and reduce the biomass particle descending velocity. Contrary to expectations, a low syrup yield and a large yield of hydrocarbon-rich gases (Table 5) were produced. Upward flowing hot pyrolysis vapors had to pass through the downward falling biomass particles before exiting the reactor. Most of the syrups condensed on the entering biomass and were recycled to the reactor. Then, secondary reactions of the recycled syrups produced more gases.

A solar pyrolysis process using orange peels in a tubular borosilicate glass reactor (external diameter of 2 inches)

Table 4

Wood pyrolysis experimental results obtained under six different heat flux densities (from Authier and L  d   (2013), Authier et al. (2009)).

Flux density (MW/m ²)	0.85	0.8	0.55	0.3	0.17	0.08
Maximum flash time (s)	6	3.33	6	13.25	18	20
Mass loss rate (kg m ⁻² s ⁻¹)	0.163	–	0.129	–	0.055	0.034
Condensable vapor yield (%)	62.3	57	62.3	61	61.7	62.0
Gas yield (%)	20.2	25	19.5	12	8.4	2.2
Char yield (%)	11.1	12	12.5	20	20.2	24.0
Mass balance (wt%)	93.6	94	94.3	93	90.3	88.2
CO (Vol%)	54.0	52.6	54.5	57.5	60.4	57.1
CO ₂ (Vol%)	13.4	13.4	15.3	18.3	18.9	22.6
H ₂ (Vol%)	14.1	17.3	14.5	6.0	3.7	–
CH ₄ (Vol%)	10.5	9.0	9.3	12.0	12.4	17.4
C ₂ H ₆ (Vol%)	0.7	0.6	0.6	0.7	0.6	0.6
C ₂ H ₄ (Vol%)	5.6	5.4	4.5	4.4	3.0	2.0
C ₂ H ₂ (Vol%)	0.9	1.0	0.6	0.3	0.4	–
C ₃ H ₈ (Vol%)	0.8	0.7	0.7	0.8	0.6	0.3

Table 5

Test results of the biomass solar pyrolysis (from Antal et al. (1983)).

Material	Cellulose	Corn Cob	Hardwood
Gasification environment	Steam	Steam	Steam
Test time (min)	18	5.5	24
Radiant flux level (MW/m ²)	0.7	0.7	0.7
Solids feed rate (g/min)	8.6	225.0	3.2
Steam flow rate (g/min)	4.3	4.3	3.5
Inert purge rate (L/min)	0.2	1.0	1.0
Exiting gas flow rate (L/min)	4.0	2.3	3.5
Solids collected (g)	184	1085	41.8
Syrups collected (g)	10.1	8.8	3.7
Gas production (L)	5.2	2.2	30.45
CO (mol%)	54.6	46.7	47.5
H ₂	20.3	13.4	21.8
CO ₂	5.8	26.1	10.9
CH ₄	12.1	8.5	13.0
C ₂ H ₄	5.7	4.7	4.3
C ₂ H ₆	0.6	0.1	0.4
C ₃ H ₈	0.3	0.3	1.8
C ₄	0.6	0.2	0.3

mounted in the focal line of a parabolic-trough solar concentrator was proposed by Morales et al. (2014). They used a Monte Carlo ray-tracing method to simulate the detailed tridimensional optical performance of the thermosolar system. The peak and average radiations of the solar reactor were 0.0251 MW/m² and 0.0126 MW/m², respectively, for 965 W/m² of direct normal irradiation (DNI). The reactor reached an average temperature of 290 °C with a peak value of 465 °C during pyrolysis. A 79 wt% sample was volatilized to 77.64 wt% liquid, 20.93 wt% char and 1.43 wt% gas. The heat balance was analyzed based on optical and thermodynamic principles. The balance indicated that the thermochemical efficiency was less than 1%. Furthermore, Zeaiter et al. designed an automated solar reactor system for the catalytic pyrolysis of scrap at 550 °C (Zeaiter, 2015). An automated sun-tracking system with two degrees-of-freedom was developed controlling both the azimuth and zenith angles via feedback from six photoresistors positioned on Fresnel lens. First, 1 g of ground scrap tire rubber pieces (3–5 mm) and 0.3 g of acidic zeolite catalyst (H-beta or H-USY) were placed in a quartz tube reactor and placed on the solar concentrator under 550 °C for 15 min. The oil and gas yields were relatively high (the highest gas yield reached 32.8%) using the H-beta catalyst, while the same results were obtained with TiO₂ or thermal pyrolysis without any catalyst. A wide distribution of C10 and C29 hydrocarbons of naphthalene and cyclohexane derivatives constituted the solar pyrolysis liquid products.

3.3. High-temperature pyrolysis using a solar furnace for gas production

A high-temperature pyrolysis process using coal was carried out in a vertical solar furnace with an increasing heat flux from 1 to 9 MW/m² (Beattie et al., 1983). The furnace consisted of a down-facing parabolic mirror (2 m diameter and 0.85 m focal length) illuminated by a reflected beam from a heliostat located beneath it. A large sliding door located below the experimental apparatus was used to block the incident radiation during shutdown. The 0.8 cm diameter coal sample (50 mg) was held in a stainless steel dish (0.8 cm diameter and 0.3 cm high) and placed in a quartz dome supported on a track. The heat flux on the sample was varied by moving the supporting track vertically so that the sample was located above or below the furnace focus. The heating time (12.5 s) was controlled by covering and uncovering the dome with an aluminum plate. The maximum devolatilization of coal (51%) occurred at a flux higher than 2 MW/m², corresponding to 1800 °C. However, a maximum gas yield of 31 mmol/g coal was obtained at a solar flux level of 1 MW/m². At fluxes lower than 1 MW/m², the ejection velocity of the primary pyrolysis vapors was lower than at higher fluxes. This lower injection velocity resulted in relatively long residence times in the high-temperature zone that enhanced the secondary reaction of the primary tar into gas. The most abundant gas was H₂, of which approximately 23.7 mmol/g coal was produced. The second most abundant gas was CO, of which approximately 4.5 mmol/g coal was produced. The hydrocarbon yield was approximately 2.37 mmol/g gas. The CO₂ yield was approximately 0.71 mmol/g coal, which increased slightly with the flux.

Thirty years after the previous study, authors from the same laboratory (CNRS, France) examined biomass pyrolysis in an improved vertical solar furnace setup (Zeng et al., 2015a, 2015b, 2015c, 2016, 2017a, 2017b, 2014, 2015; Li et al., 2016; Soria et al., 2017). The most important improvement was the ability to control the heating rate and plateau temperature of biomass using a shutter. Fig. 9 shows the improved experimental setup. The maximum power and flux density were approximately 1.5 kW and 12000 kW/m², respectively. A shutter with moving blades composed of a carbon composite modulated the reflected solar beam, which, in turn, modulated the incident radiation and the concentrated flux impinging the sample and its temperature. A transparent Pyrex balloon reactor with a 185 mm diameter (6 L volume), set at the focus, was swept with argon flow controlled by a mass flowmeter (Bronkhorst, EL-FLOW[®]). The sweep gas was used to keep the reactor wall and fluorine window clean. A needle valve adjusted the reactor outlet gas flow, which eventually controlled the reactor pressure. The sample surface temperature was measured using a “solar-blind” optical pyrometer (a KLEIBER monochromatic pyrometer operating at 5.2 μm). The target heating rate and final temperature were set using a PID controller, which controlled the shutter opening based on the measured sample temperature. The pyrolysis products (condensable vapors and incondensable gases) first circulated through a 250 °C heated copper tube (to avoid unwanted deposition before collection). Then, they passed through a dry ice condensation train composed of three impinger bottles immersed in dry ice (with temperatures between approximately –25 °C and –15 °C). Each bottle contained approximately 100 ml of isopropanol (2-propanol) as a solvent to achieve a higher tar capture efficiency and for further CHNS, Karl-Fischer titration and GC–MS analyses. A needle valve and a vacuum pump were set downstream from the condensation train. The permanent gases were collected in a sampling bag through the vacuum pump. Afterwards, the outlet gas composition was determined using gas chromatography (SRA Instruments MicroGC 3000). CHNS analysis, scanning electron microscopy analysis,

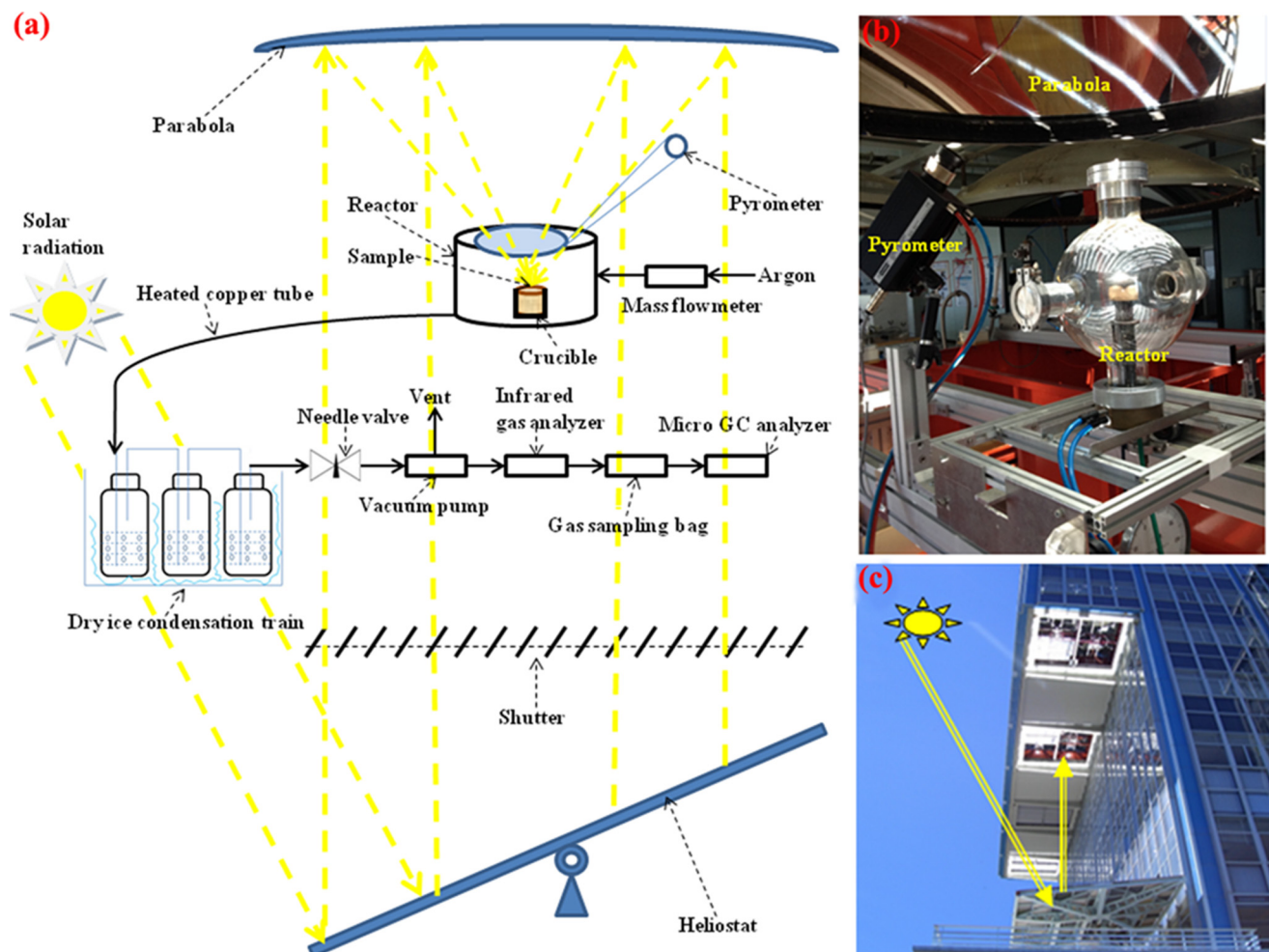


Fig. 9. Schematic of the solar pyrolysis experimental setup: (a) whole system, (b) solar reactor and (c) vertical solar furnace (from Zeng et al. (2017b)).

X-ray diffractometry, and Brunauer–Emmett–Teller adsorption experiments were employed to investigate the composition and structure of the char left in the crucible.

There were two characteristic sections in the solar reactor: (1) the two temperature zones, depicted in Fig. 10a, and (2) the rotational flow field, shown in Fig. 10b (Zeng et al., 2015b). As shown in Fig. 10a, the wood pellet was placed in a graphite crucible and wrapped with black graphite foam. It was directly heated using solar radiation. Argon did not absorb the solar radiation because it is transparent in this wavelength region. Thus, it could only be heated due to contact with the sample surface or by convection mixing with the volatile pyrolysis products. Because the sides and bottom of the sample were insulated with graphite foam, the zone near the sample top surface was a high-temperature zone. The remaining zones in the solar reactor remained relatively cold compared to the crucible. Consequently, the secondary tar reactions could only occur in the high-temperature zone. The argon injection system was composed of six upward holes (near the reactor gas outlet) and six downward holes (on the side opposite of the gas outlet) in a circular tube to promote mixing (the effect of counter-current argon injection on flow field is schemed in Fig. 10b).

Beech wood pellets (approximately 0.3 g), which were 10 mm in diameter and 5 mm high, were used in the experiments. The beech wood characteristics are shown in Table 6. The experiments consisted of two steps as follows: (1) a one-factor-at-a-time (OFAT) approach and (2) a response surface methodology (RSM). First, the influences of the single factors, temperature (600–2000 °C), heat-

ing rate (5–450 °C/s), pressure (0.48–1.18 bar) and argon flow rate (6–12 NL/min), on the product distributions were determined (Zeng et al., 2015b, 2014, 2015). Then, the combined effects of the temperature (800–2000 °C), heating rate (50–450 °C/s) and argon flow rate (4–8 NL/min) were investigated. The gaseous products were characterized to determine the optimum parameters required to maximize the LHV (lower heating value) of the gas products (Zeng et al., 2015c). In addition, the coproducts, biochars and bio-oils obtained from these experiments were characterized (Zeng et al., 2015a). Finally, for the first time, the energetic upgrade factor of the solar pyrolysis process was determined (Zeng et al., 2017a). The influence of the biomass species (Li et al., 2016) and their initial water content (Zeng et al., 2017b) has also been investigated.

3.3.1. Effect of the heating parameter

The temperature drastically affects the final product distribution and gas composition during solar pyrolysis; hence, it is the key parameter that governs solar pyrolysis reactions. A maximum gas yield of 63.1% was obtained at a temperature of 1600 °C while the liquid and char yields decreased to 28.8% and 8.4%, respectively (Fig. 11). The molar yields of H₂ and CO significantly increased from 0 to 15 mol/kg of wood and from 4.08 to 17.55 mol/kg of wood, respectively, as the temperature increased from 600 to 1600 °C. The total gas product lower heating values increased 5-fold, from 1878 ± 75 to 9621 ± 305 kJ/kg of wood, as the temperature increased from 600 to 1200 °C. The molar ratio between H₂

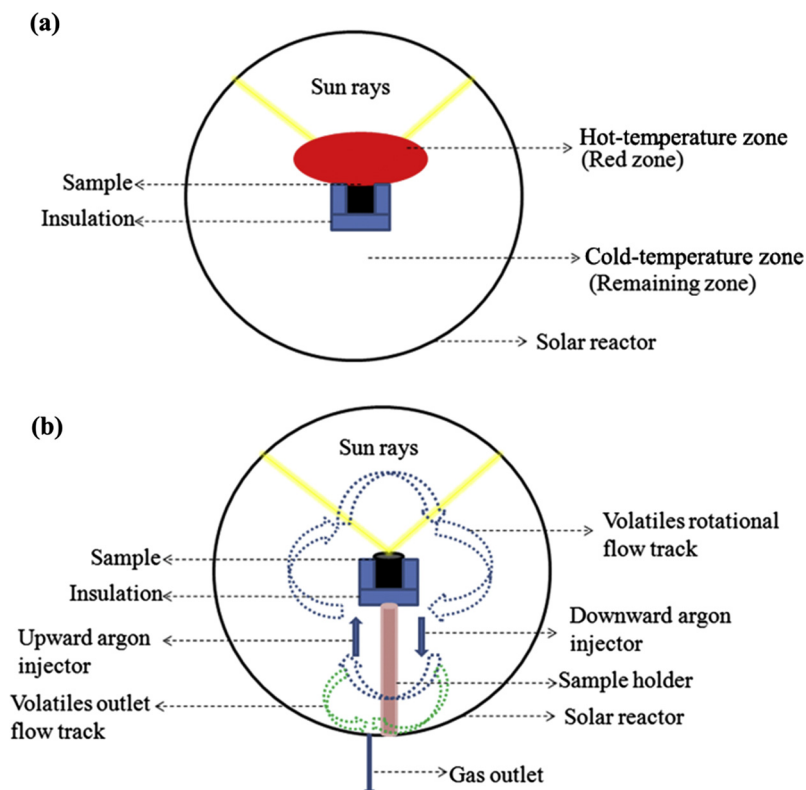


Fig. 10. Solar reactor characteristics: (a) two temperature zones and (b) rotational flow field (from Zeng et al. (2015b)).

Table 6

The main properties of beech wood (from Zeng et al. (2015b)).

Proximate analysis				Ultimate analysis				
Volatile matter	Fixed carbon	Ash	Moisture	C	H	O	N	S
%mass, dry				%mass				
85.3	14.3	0.4	6	50.8	5.9	42.9	0.3	0.02

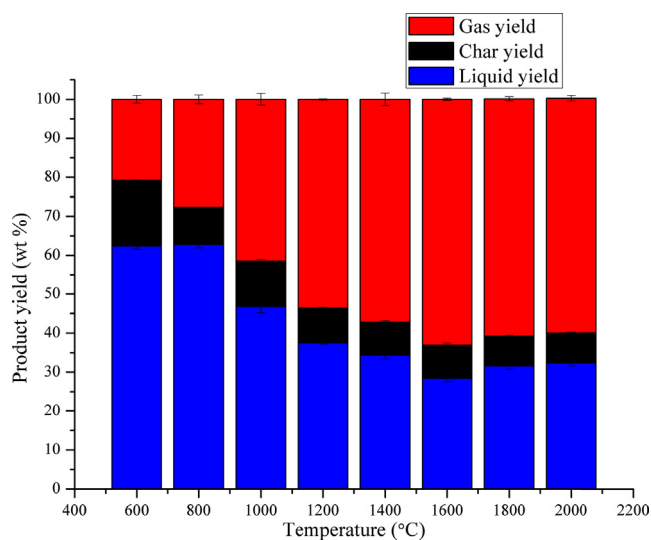


Fig. 11. Product yield as a function of temperature (pyrolysis conditions: heating rate of 50 °C/s, pressure of 0.44 bar, and argon flow rate of 6 NL/min) (data from Zeng et al. (2015b)).

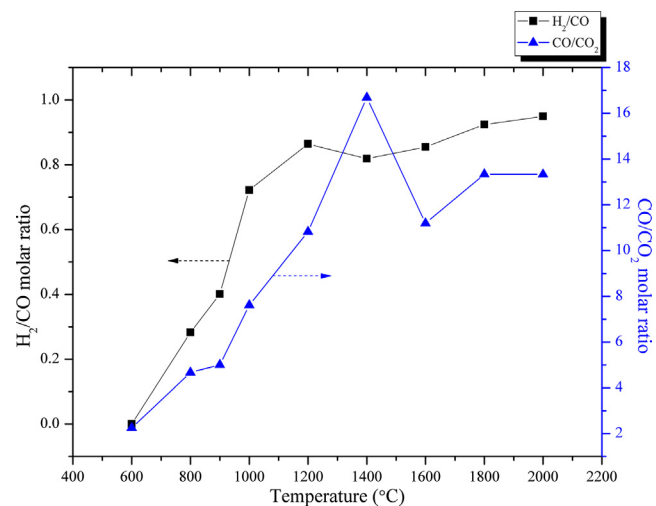


Fig. 12. H₂/CO and CO/CO₂ molar ratios as a function of temperature (pyrolysis conditions: heating rate of 50 °C/s, pressure of 0.44 bar, and argon flow rate of 6 NL/min) (data from Zeng et al. (2015b)).

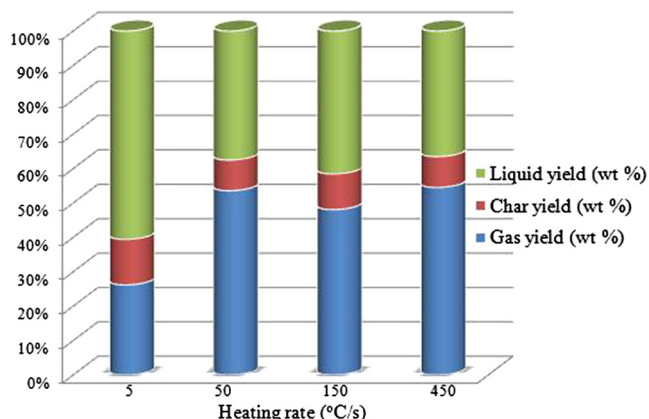


Fig. 13. Product yield as a function of the heating rate (pyrolysis conditions: temperature of 1200 °C, pressure of 0.44 bar, and argon flow rate of 6 NL/min) (data from Zeng et al. (2015b)).

and CO increased from 0 to 0.95 when the temperature increased from 600 to 2000 °C, as presented in Fig. 12. Meanwhile, the CO/CO₂ ratio first increased from 2.25 to 16.69 when temperature increased from 600 to 1400 °C. Then, it decreased to 13.33 at higher temperatures. As the heating rate increased from 5 to 50 °C/s, the liquid and char yields substantially decreased from 60.6% to 37.5% and from 13.2% to 8.9%, respectively, whereas the gas yields sharply increased from 26.2% to 53.6% (Fig. 13). The CO and H₂ yields remarkably increased from 5.78 to 14.29 mol/kg of wood and from 2.75 to 12.35 mol/kg of wood, respectively when the heating rate increased from 5 to 50 °C/s. The total lower heating values of the gases remarkably increased from 3386 to 9621 kJ/kg of wood as the heating rate increased from 5 to 50 °C/s. The H₂/CO and CO/CO₂ ratios increased from 0.46 to 0.86 and 3.5 to 10.3, respectively, as the heating rate increased from 5 to 50 °C/s, as shown in Fig. 14. The change of the product distribution and gas composition was due to the enhanced tar and char secondary reactions at high temperatures and fast heating rates. The sweep gas flow rate and pressure had a minimal influence on the solar pyrolysis product distribution.

3.3.2. Effect of the biomass characteristics

Different biomass feedstocks (pine sawdust, peach pit, grape stalk and grape marc) were pyrolyzed using the same solar reactor.

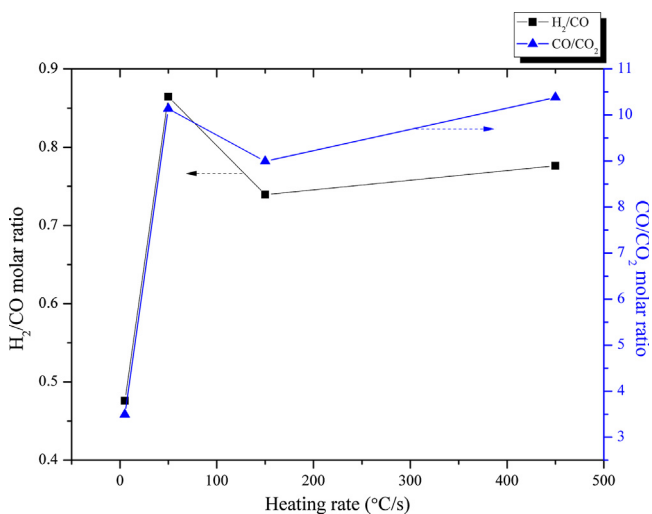


Fig. 14. H₂/CO and CO/CO₂ molar ratios as a function of the heating rate (pyrolysis conditions: heating rate of 50 °C/s, pressure of 0.44 bar, and argon flow rate of 6 NL/min) (data from Zeng et al. (2015b)).

Both of grape byproducts containing more lignin than that of peach pits and pine sawdust produced higher char yields and lower gas yields (Li et al., 2016). Because lignin pyrolysis tends to form more char than that of cellulose and hemicellulose under the same conditions (Fahmi et al., 2008). Beech wood sawdust with initial water contents 0%, 6%, 11% and 41% were pyrolyzed in a solar reactor at 900, 1200 and 1600 °C with heating rates ranging from 10 to 150 °C/s (Zeng et al., 2017b). Fig. 15 show the plots of the effects of the initial water content on the product distributions and gas characterization at a pyrolysis temperature of 1200 °C and heating rate of 50 °C/s. As shown in Fig. 15a (pyrolysis at 1200 °C), the liquid yield (with error bars) remained almost constant at approximately 41.8% when the water content increased from 0% to 41%. Meanwhile, the gas yield increased from 47.8% to 53.8%, and the char yield decreased from 10.4% to 5.7%. According to Fig. 15b, the CO and H₂ molar yields increased from 11.8 to 12.5 mol/kg of wood and from 9 to 11.8 mol/kg of wood, respectively with the water content increased from 0% to 41%. These increases were mainly due to the promoted steam gasification with char (Karayildirim et al., 2006). The CH₄ and C₂H₆ yields slightly decreased monotonically with the increasing water content, because of the enhanced reactions (Blasi et al., 2015). The CO₂ increased at the expense of CH₄.

3.3.3. Characterization of the products

The properties of char products are influenced by the solar pyrolysis temperature and heating rate. The degree of char carbonization increases with the temperature while decreases with the heating rate (when higher than 50 °C/s). The BET surface area and pore volume first increase when the temperature increases from 800 to 1200 °C, then decreases at higher temperatures (Zeng et al., 2015a). They first increase with a heating rate peak of approximately 150 °C/s and then decrease at 450 °C/s when temperature is higher than 1200 °C (Zeng et al., 2015a). The larger the BET surface area and pore volume of the char are, the higher the char reactivity is, which means that these parameters are good indicators of the char reactivity. The solar pyrolysis bio-oil properties are presented in Table 7 (Zeng et al., 2017a). Temperature has no obvious influence on the water content and element concentrations of solar pyrolysis bio-oil. The lower water content of solar pyrolysis bio-oil than conventional pyrolysis bio-oil may be explained by the water consumed during gasification reactions at higher temperatures. Nevertheless, it is uncertain whether the water content can condense on the water-cooled parts of the reactor before reaching the sampling line. Consequently, the energy upgrade factor is given as a function of the water content in the range 0–30 wt% (Section 3.3.4). The carbon content was approximately 58%, and the oxygen content in the bio-oil was lower than that in the feedstock since the O content was split between the NCG gases (CO₂ and CO) through pyrolysis (Mullen et al., 2010). The hydrogen content in solar pyrolysis bio-oil is about twice as high as that in conventional pyrolysis bio-oil. The low oxygen and high hydrogen contents make solar pyrolysis bio-oil an attractive fuel (Huber et al., 2006).

The C, H, N and S contents of char and bio-oil have been directly determined using CHNS analyses. The LHVs (lower heating values) for gas, char and oil have been determined using empirical equations (Channiwal and Parikh, 2002; Gaur and Reed, 1995). The calculated HHVs and LHVs for solar pyrolysis bio-oils obtained at temperatures of 600 and 900 °C were approximately 31 and 30 MJ/kg, respectively, and increased to 33 and 32 MJ/kg for temperatures of 1200 and 2000 °C, respectively, due to the hydrogen content increase with temperature. The gas energy contribution greatly increased with temperature. However, the bio-oil and char energy contribution slightly decreased with temperature. The bio-oil energy contributed more than 50% of the total energy

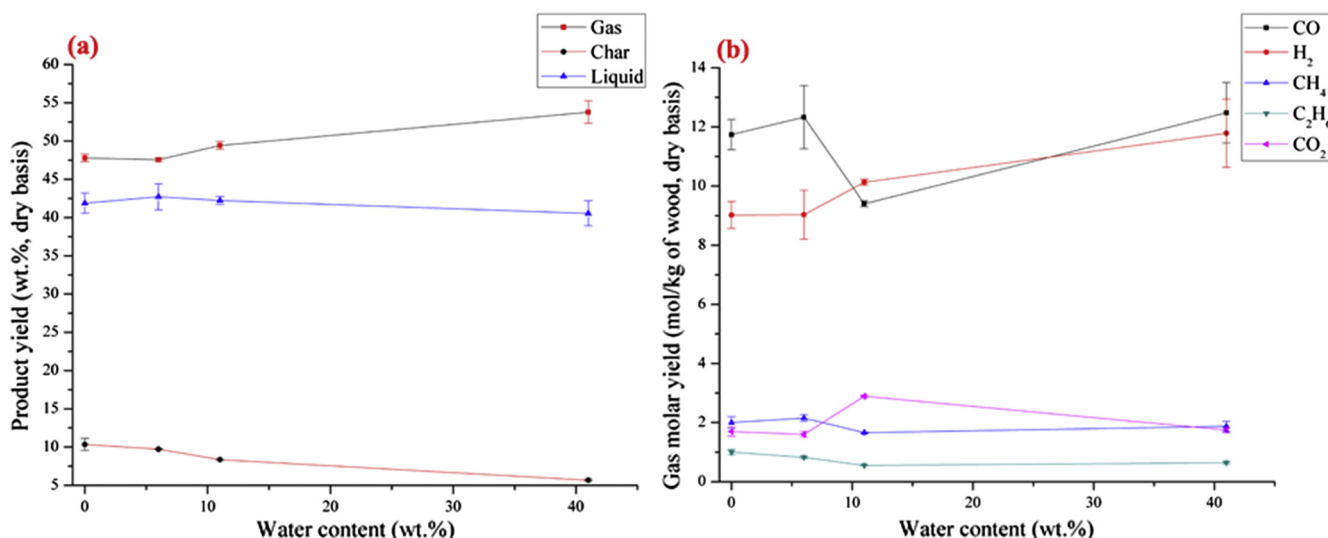


Fig. 15. Effects of the initial water content on the solar pyrolysis of biomass: (a) product distribution, (b) gas composition (temperature of 1200 °C and heating rate of 50 °C/s) (data from Zeng et al. (2017b)).

Table 7

Properties of the solar pyrolysis bio-oil (from Zeng et al. (2017a)).

Composition	600 °C bio-oil	900 °C bio-oil	1200 °C bio-oil	2000 °C bio-oil	Typical bio-oil (Dickerson and Soria, 2013)	Crude oil (Dickerson and Soria, 2013)
Water (wt%)	1.43	1.67	1.51	1.15	15–30	0.1
Density (kg/L)	–	–	–	–	1.05–1.25	0.86–0.94
Viscosity 50 °C (cP)	–	–	–	–	40–100	180
HHV (MJ/kg of tar)	30.74	30.73	33.24	33.11	16–19	44
LHV (MJ/kg of tar)	30.26	30.18	32.7	32.7	–	44
C (wt%)	58.1	57.4	58.8	58.6	55–65	83.86
O (wt%)	30.16	30.61	27.7	27.88	28–40	<1
H (wt%)	11.37	11.61	13.08	13.04	5–7	11–14
S (wt%)	0.0826	0.0835	0.0357	0.0658	<0.05	<4
N (wt%)	0.37	0.38	0.42	0.48	<0.4	<1
Ash (wt%)	–	–	–	–	<0.2	0.1
H/C	2.35	2.43	2.67	2.67	0.9–1.5	1.5–2.0
O/C	0.39	0.4	0.35	0.36	0.3–0.5	~0

Table 8

Energy upgrade factor comparison.

Process	Feedstock	Upgrade factor	Method	Reference
Conventional autothermal gasification	Coal	0.65	Calculation	Chueh et al. (2010)
Conventional autothermal pyrolysis	Forest waste	0.91	Calculation	Daugaard and Brown (2003)
Solar gasification	Biomass	1.188	Calculation	Nzihou et al. (2012)
Solar gasification	Beech charcoal	1.3	Experiment	Piatkowski et al. (2009)
Solar pyrolysis	Beech wood	1.21–1.38–1.53 ^a	Experiment	Zeng et al. (2017a)

^a Assuming 30, 15 and 1.5 wt% water respectively.

production at all of the temperatures. At high temperatures of 1200 and 2000 °C, the gas energy contributions were almost the same as those of tar.

3.3.4. Evaluation of the energy upgrade factor

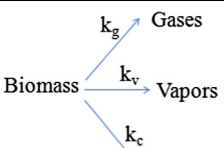
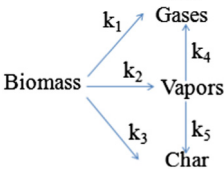
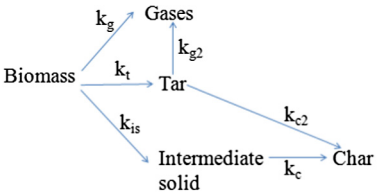
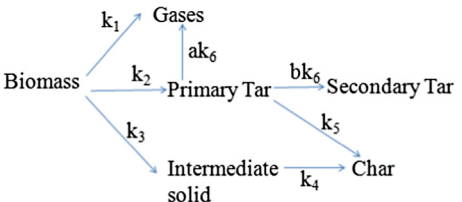
The energy upgrade factor of the solar pyrolysis process is defined as the ratio of the sum of the produced bio-oil, gas and bio-char lower heating values over the lower heating value of the feedstock, as shown in Eq. (2). Both the measured and the estimated energy upgrade factors of solar pyrolyzed biomass at different temperatures were determined. The total product energy content was calculated based on the LHV of the as-measured solar bio-oil (negligible water content, see Table 7) and the LHV assuming water contents of 15% and 30% (which is the typical water content range

of standard bio-oil) to represent the possible the upper limit, mean value and lower limit. The energy upgrade factors increased from 1.14–1.33–1.49 to 1.21–1.38–1.53, respectively, when the temperature increased from 600 to 900 °C. Then, they slightly decreased to 1.21–1.33–1.44 at 1200 °C and, more significantly, to 1.18–1.28–1.37 at 2000 °C. The variations of the energy upgrade factor were mostly due to the bio-oil yield decrease with temperature. The biomass energy upgrade factors, U, for conventional autothermal pyrolysis, conventional autothermal gasification, solar gasification and solar pyrolysis processes are compared in Table 8. U values greater than 1 for the solar gasification/pyrolysis processes indicated successful solar energy storage as chemical energy and the achievement of upgrading the fuel calorific value. In contrast, conventional autothermal pyrolysis and gasification upgrade

Table 9
Summary of the reactors developed for solar pyrolysis of carbonaceous feedstocks and their associated results.

Reference	Reactor design			Radiation concentrator	Heating source	Incident flux	Feedstock		Product distribution (wt.)		
	Variety	Shape	Dimensions				Variety	Size	Solid	Liquid	Gas
Hopkins et al. (1984), Antal et al. (1980)	Spouted bed	Cylinder	22 mm i.d.	2 parabolic mirrors, 24 flat glass mirrors	5 kW Xenon lamp	2 MW/m ²	Cellulose Kraft paper 2–8 g	Particles with μm diameters	11% 15%	63% 30%	26% 55%
Hopkins et al. (1984)	Fixed bed	Cylinder	–	Polished cylindrical aluminum reflector	Helical Xenon flash lamp	80 MW/m ²	Biomass	A few tens of milligrams of particles	–	25%	32%
Tabatabaie-Raissi and Antal (1986), Tabatabaie-Raissi et al. (1989)	Fixed bed (TGA)	Cylinder	35 mm o.d. and 640 mm long tube	2 parabolic mirrors, 24 flat glass mirrors	2 kW Xenon lamp	Up to 10 MW/m ²	Cellulose	Particles with μm diameters	6.6–8.4%	–	–
Hunjan et al. (1989)	Fixed bed	Cylinder	399 cm ³	1 ellipsoidal mirror	1 kW arc lamp	1 MW/m ²	Acetone	Gas phase	–	–	–
Antal et al. (1983), Boutin et al. (1998)	Fixed bed	Dome-like cylindrical with quartz window	–	–	1 kW Xenon arc lamp	0.083, 0.167 and 0.25 MW/m ² (150–900 °C)	Pine	Pellet (diameter, 10 mm; thickness, 5, 10 and 15 mm)	20–26%	33–52%	11–27%
Grønli and Melaen (2000), Grønli (1996)	Fixed bed	Bell-shaped Pyrex reactor	–	Reflector	Xenon lamp	0.08 and 0.13 MW/m ² (150–970 °C)	Birch, pine, and spruce ~5 g	Pellet (diameter, 20 mm; thickness, 30 mm)	21–29%	25–40%	30–50%
Boutin et al. (2002)	Fixed bed	Cylinder with conical parts at its bottom and top	30 mm o.d. and 50 mm long tube	2 parabolic mirrors	5 kW Xenon lamp	0.2–4, 5 and 7.4 MW/m ²	Cellulose	Pellets with a circular cross section of 0.2 cm ²	–	–	–
Authier et al. (2009)	Fixed bed	Cylinder	30 mm o.d. and 50 mm long tube	2 parabolic mirrors	5 kW Xenon lamp	0.3–0.8 MW/m ²	Oak 0.125 g	Pellet (radius, 5 mm; thickness, 3 mm)	20%	61%	12%
Authier and Lédé (2013)	Fixed bed	Cylinder	30 mm o.d. and 50 mm long tube	2 parabolic mirrors	5 kW Xenon lamp	0.08, 0.17, 0.55 and 0.85 MW/m ²	Oak 0.13 g	Pellet (radius, 5 mm; thickness, 3 mm)	11.1–24%	61.7–62.3%	2.2–20.2%
Pozzobon et al. (2014)	Fixed bed	–	–	2 elliptical mirrors	0.75 kW tungsten lamp	0.06, 0.09, 0.12, 0.15 and 0.18 MW/m ²	Beech	Cylinder (diameter, 5 mm; height, 5 mm); Sphere (10 and 20 mm diameter)	9–13%; 14–20%	–	–
Morales et al. (2014)	Fixed bed	Tubular reactor	50.8 mm diameter and 406.4 mm length	Parabolic-trough concentrator	Sun (15.65 suns)	0.01255 MW/m ² (average reactor temperature 290 °C, peak temperature 465 °C)	Orange peel	Particle sizes of 20 mm × 20 mm × 3 mm and 30 mm × 3 mm	21%	77.6%	1.4%
Zeaiter (2015)	Fixed bed	Tubular reactor	200 mm long with small diameter	Fresnel lens	Sun	– (average reactor temperature 550 °C)	Scrap rubber 1 g	3–5 mm ground pieces	42%	28%	30%
Zeng et al. (2015a, 2015b, 2015c, 2016, 2017a, 2017b, 2014, 2015), Li et al. (2016), Soria et al. (2017)	Fixed bed	Balloon reactor	185 mm diameter (6 L volume)	Parabolic mirror (2 m diameter)	Sun	Up to 12 MW/m ² (Up to 2000 °C)	0.3 g	10 mm in diameter, 5 mm in height pellet	8%	29%	63%

Table 10
Kinetic pathways of the solar pyrolysis models.

Kinetic Scheme	Arrhenius law	Reference
	$k = A_i \exp(-E_i/RT)$ $i = \text{gas, vapor, char}$	Al-Haddad et al. (2010)
	$k = A_i \exp(-E_i/RT)$ $i = 1, 2, 3, 4, 5$	Kenarsari and Zheng (2014)
	$k = A_i \exp(-E_i/RT)$ $i = \text{gas, tar, intermediate solid, char, gas2, char2}$	Pozzobon et al. (2014)
	$k = A_i \exp(-E_i/RT)$ $i = 1, 2, 3, 4, 5, 6$	Zeng et al. (2016)

factors were less than 1 due to burning a portion of the feedstock for providing the reaction heat. Indeed, conventional autothermal pyrolysis and gasification require the internal combustion of some portion of the injected feedstock mass with air in order to supply process heat for the endothermic reactions. For example, on a dry basis, 1.6 ± 0.3 MJ/kg was necessary for pyrolyzing pine wood with an LHV of 17.9 MJ/kg at approximately 500 °C (Daugaard and Brown, 2003). Therefore, at least 9 wt% of the injected biomass must be burned separately to power the reaction, which inherently decreases the biomass valorization. For bituminous coal (LHV = 34 MJ/kg), 12 MJ/kg was required for its steam gasification. Thus, at least 35 wt% of the coal must be burned for providing the required heat of reaction (Piatkowski et al., 2011).

$$U = \frac{m_{oil}LHV_{oil} + m_{gas}LHV_{gas} + m_{char}LHV_{char}}{m_{feedstock}LHV_{feedstock}} \quad (2)$$

3.4. Summary of the solar pyrolysis prototypes

A very high heat flux density can be reached quickly with concentrated solar radiation under very clean conditions. Fast heating rates and high temperatures can be obtained with a well-controlled heating time during the solar pyrolysis process. Only the radiation-absorbing feedstock is heated, not the reactor wall and sweeping gas. Moreover, the thermal conditions (temperature and heating rate) imposed on the solid can be varied independently of the sweep gas and reactor (Antal et al., 1983). A summary of the main characteristics of pyrolysis under concentrated radiation is presented in Table 9. Several prototypes have been designed based on conventional reactor knowledge, including gas-solid chemical reactors in which reactants directly absorb the radiation.

4. Solar pyrolysis modeling

Numerical simulations of free-falling (countercurrent) and entrained (co-current) flow solar fired biomass flash pyrolysis reactors were carried out by Hofmann and Antal (1984), Antal et al. (1983). They used finite-difference methods (FDM) to divide the reactor length into n segments and derived equations along the reactor length based on mass/energy conversions and rate laws for pyrolysis and heat transfer. Gas flows within the solar reactor were arranged to secure longer solid residence times in the zone of intense radiant energy. The predicted residence times required to achieve complete pyrolysis were strongly dependent on the chosen pyrolysis rate law. The simulations confirm the importance of identifying the accurate solar pyrolysis rate law through dedicated experiments. Pyrolysis kinetic parameters (rate laws) depend on the heating rate and final temperature reached (Liang et al., 2014; Vamvuka and Sfakiotakis, 2011; Haykiri-Acma et al., 2006). They play an important role in determining the pyrolysis product distribution (Blasi, 1993, 2008; Akhtar and Amin, 2012; Neves et al., 2011). Understanding the kinetics of solar pyrolysis processes and accurately predicating pyrolysis rates are of great importance for the optimal design of solar pyrolysis reactors.

The simple kinetic pathways derived from the “Broido-Shafi zadeh” model were validated using flash pyrolysis with cellulose pellets submitted to concentrated radiation (Boutin et al., 2002). Three parallel reaction schemes, considering char, tar and gas, were used for biomass pyrolysis in an image furnace (Authier et al., 2009; Al-Haddad et al., 2010). Under such conditions, condensable vapors released from the biomass were immediately quenched. Secondary tar reactions were not considered in such models. However, the primary pyrolysis products (vapors and gases) were produced during secondary reactions if their residence time was sufficiently long in the high-temperature zone.

Table 11
Governing equations of the solar pyrolysis models.

Reference	Al-Haddad et al. (2010)	Kenarsari and Zheng (2014)	Pozzobon et al. (2014)	Zeng et al. (2016)
Solid masses	$\frac{dC_s}{dt} = -\left(\frac{dC_s}{dt} + \frac{dC_g}{dt} + \frac{dC_c}{dt}\right)$	$\frac{\partial \theta}{\partial t} = \omega_1$	$\frac{dC_B}{dt} = -(k_1 C_B + K_2 C_B + K_3 C_B)$ $\frac{dC_C}{dt} = k_3 C_B + k_5 C_V$	$\frac{\partial \rho_w}{\partial t} = -(k_1 + k_2 + k_3) \rho_w$ $\frac{\partial \rho_s}{\partial t} = k_3 \rho_w - k_4 \rho_s$ $\frac{\partial \rho_c}{\partial t} = k_4 \rho_s + \varepsilon k_5 \rho_{t1}$
Gas phase masses	$\frac{dC_g}{dt} = A_1 e^{-\varepsilon_1 / k_g T} C_w(t)$	$\rho g = \frac{NM_k \xi}{RT}$	$\frac{dC_V}{dt} = k_2 C_B - K_5 C_V - K_4 C_V$ $\frac{dC_W}{dt} = k_1 C_B + K_4 C_V$	$\frac{\partial(\rho_{Ar})}{\partial t} + \frac{\partial}{\partial x}(\rho_{Ar} v_x - \frac{\partial(D\rho_{Ar})}{\partial x}) + \frac{1}{T} \frac{\partial}{\partial t} (r \rho_{Ar} v_r - r \frac{\partial(D\rho_{Ar})}{\partial r}) = 0$ $\frac{\partial(\rho_{O_2})}{\partial t} + \frac{\partial}{\partial x}(\rho_{O_2} v_x - \frac{\partial(D\rho_{O_2})}{\partial x}) + \frac{1}{T} \frac{\partial}{\partial t} (r \rho_{O_2} v_r - r \frac{\partial(D\rho_{O_2})}{\partial r}) = S_{g2}$ $S_g = k_1 \rho_w + \varepsilon k_5 \rho_{t1}$ $\frac{\partial(\rho_{H_2O})}{\partial t} + \frac{\partial}{\partial x}(\rho_{H_2O} v_x - \frac{\partial(D\rho_{H_2O})}{\partial x}) + \frac{1}{T} \frac{\partial}{\partial t} (r \rho_{H_2O} v_r - r \frac{\partial(D\rho_{H_2O})}{\partial r}) = S_{t1}$ $S_{t1} = k_2 \rho_w - \varepsilon(k_5 + k_6) \rho_{t1}$ $\frac{\partial(\rho_{CO_2})}{\partial t} + \frac{\partial}{\partial x}(\rho_{CO_2} v_x - \frac{\partial(D\rho_{CO_2})}{\partial x}) + \frac{1}{T} \frac{\partial}{\partial t} (r \rho_{CO_2} v_r - r \frac{\partial(D\rho_{CO_2})}{\partial r}) = S_{t2}$ $S_{t2} = \varepsilon k_6 \rho_{t1}$
Energy	$\frac{\partial(\rho C_p T)}{\partial t} = \lambda_1 \left(\frac{\partial T}{\partial r} + \frac{1}{r} \frac{\partial T}{\partial r} \right) + \lambda_2 \frac{\partial T}{\partial z} - \sum_i (\Delta H_i) \left(\frac{dC_i}{dt} \right)$	$(\rho C_p)_{eq} \frac{\partial T}{\partial t} + \rho_g C_{p,g} \nabla \cdot (\vec{u} T) = -\nabla \cdot (-\lambda_{eff} \nabla T) + Q$	$\frac{\partial(\rho C_p T)}{\partial t} = \lambda \left(\frac{\partial^2 T}{\partial r^2} + \frac{1}{r} \frac{\partial T}{\partial r} + \frac{\partial^2 T}{\partial x^2} \right) + \sum_j (-\Delta H_j) \left(\frac{-\partial C_j}{\partial t} \right)$	$(\rho_w C_{p,w} + \rho_s C_{p,s} + \rho_c C_{p,c} + \rho_{t1} C_{p,t1} + \rho_{t2} C_{p,t2} + \rho_g C_{p,g}) \frac{\partial T}{\partial t} + \frac{\partial(\rho_g C_{p,g} v_r T)}{\partial x} = \frac{\partial}{\partial x} (\lambda_{eff(x)} \frac{\partial T}{\partial x}) + \frac{\partial}{\partial r} \left(r^2 \frac{\partial T}{\partial r} \right) + Q$
Heat generation	-	$Q = -\sum \Delta H_i \omega_i$	-	$Q = -(k_1 \Delta H_1 + k_2 \Delta H_2 + k_3 \Delta H_3) \rho_w - k_4 \Delta H_4 \rho_s - \varepsilon(k_5 \Delta H_5 + k_6 \Delta H_6) \rho_{t1}$

Thus, biomass pyrolysis should be described using a primary stage and a secondary stage (Chan et al., 1985; Grønli and Melaaen, 2000; Blasi, 1996). Chan et al. (1985) developed a mathematical model for wood pyrolysis under radiation that included water release, tar cracking and char deposition chemical reactions that can be used for predicting the ultimate product distribution. Blasi (1996) developed a coupled transport and reaction model for biomass pyrolysis heated by radiation. The simulation results of wooden particles subjected to specific external radiation revealed that the secondary tar reactions were enhanced with the heat flux. Grønli et al. presented a competitive reaction model that included a secondary tar cracking step, which could be used to predict the effects of heat flux on the product distribution during biomass pyrolysis (Grønli and Melaaen, 2000). Recently, a few researchers developed particle models to study the effects of the process parameters, such as the radiant heat flux from an image furnace, on the product distribution of biomass pyrolysis (Pozzobon et al., 2014; Al-Haddad et al., 2010; Kenarsari and Zheng, 2014). The first CFD model to investigate the effects of process parameters (temperature and heating rate) on the product distribution of biomass pyrolysis in a real solar reactor was proposed in Zeng et al. (2016), Soria et al. (2017). The kinetic schemes and the governing equations for these four solar pyrolysis particle models are listed in Tables 10 and 11.

The experimental results indicated that the char and vapor yields decreased (from 21 ± 2 to 12 ± 1 wt% and from 63 ± 6 to 49 ± 6 wt%) when the mean available heat flux density increased from 0.2 to 0.8 MWm⁻², whereas the gas yields increased from 9 ± 1 to 36 ± 2 wt% (Al-Haddad et al., 2010). Considering the secondary tar reactions, the simulated results demonstrated were more consistent with the experimental data, as presented in Table 12 (Kenarsari and Zheng, 2014). This result proves that secondary reactions should be considered in solar pyrolysis modeling, especially when the pyrolysis time is relatively long. Considering char steam gasification from water vapor due to a drying feedstock, numerical predictions successfully captured the trends and values of the final char yield for different heat fluxes (Fig. 16) (Pozzobon et al., 2014). This model evidenced the presence of a drying front prior to the pyrolysis front, which led to steam release during the drying step that diffused through the high-temperature char matrix and reacted with it. Both the temperature and heating rate could be used to influence and determine the proportions of the main products of the solar pyrolysis process and their characteristics. Most models of pyrolysis under concentrated radiation have been developed based on experimental results obtained under low heating rates (Chan et al., 1985; Grønli and Melaaen, 2000; Authier et al., 2009; Pozzobon et al., 2014; Blasi, 1996; Kenarsari and Zheng, 2014). Actually, solar pyrolysis has the advantages of high temperatures and fast heating rates. The reaction rate constants depend on the heating rate (Van de Velden et al., 2010). Therefore, a selection of kinetic equations based on fast heating rate experimental tests were proposed for modeling solar pyrolysis under severe conditions (heating rates reaching 450 °C/s and temperatures reaching 2000 °C) in the present authors' simulation (Zeng et al., 2016). The product distribution from model was validated against experimental data obtained from solar pyrolysis experiments under two different heating rates, 10 and 50 °C/s, and five final temperatures, 600, 900, 1200, 1600 and 2000 °C (Fig. 17). After, a comprehensive CFD model capable of predicting the pyrolysis behavior (not only the char, tar and gas yields but also the species compositions of the two latter products) for a wide range of feedstocks and operating conditions was developed in Soria et al. (2017). The gas composition calculated according to the comprehensive model was also validated (Fig. 18).

Table 12
Solar pyrolysis product yields (oak) (from Kenarsari and Zheng (2014)).

Incident radiant heat flux (MW/m ²)	Times (s)	Gases (wt%)	Vapors (wt%)	Char (wt%)	
$\phi = 0.3$	13.25	9.3	69.3	21.4	Simulation (Kenarsari and Zheng, 2014)
		8.4	61.6	22.9	Experimental data (Authier et al., 2009)
$\phi = 0.8$	3.33	17.8	69.9	12.3	Simulation (Kenarsari and Zheng, 2014)
		21.7	62.5	11.2	Experimental data (Authier et al., 2009)

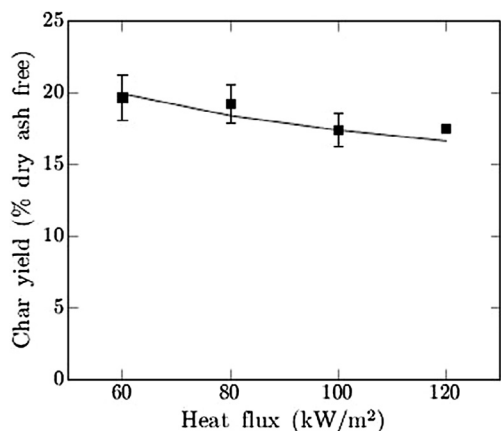


Fig. 16. Final char yield versus the heat flux (from Pozzobon et al. (2014)). Square = experimental observations and solid line = numerical predictions.

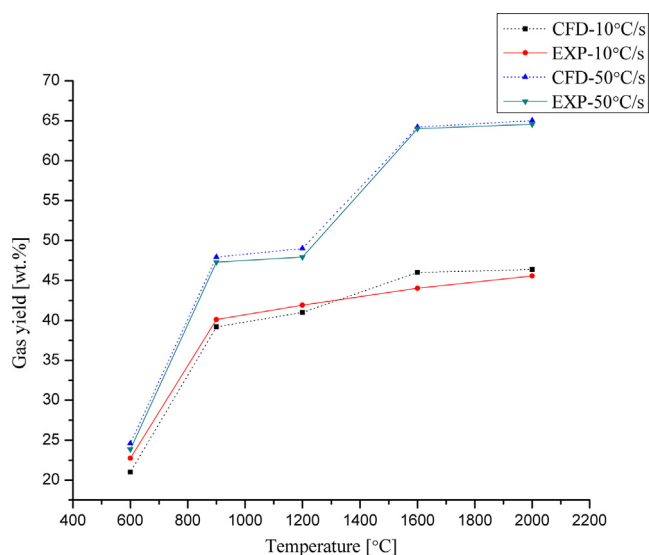


Fig. 17. Gas yield: comparison between the CFD model prediction values and experimental results (from Zeng et al. (2016)).

5. Challenges for solar pyrolysis

The solar pyrolysis of carbonaceous feedstocks has been successfully demonstrated at the laboratory scale in directly heated reactors; however, no pilot scale demonstration is available, in contrast to solar gasification (Wieckert et al., 2013). The challenges for solar pyrolysis processes are both technical and economic. The technical challenges include the type, material, scale up and operation of the solar reactor. The primary economic challenge is the

capital cost of the installed heliostats. The main issues of the solar pyrolysis process are described below:

(a) How does one choose the solar reactor type?

Two main basic designs are possible: indirect and direct feed-stock heating. In the former, the carbonaceous feedstock is heated either by radiation and convection from the reactor walls or by an intermediate heat transfer fluid (HTF). One of the best options for the HTF is an inert particle flow that carries solar heat from the receiver subsystem to the reactor subsystem, as proposed in Nzihou et al. (2012). In this concept, the inert particles are heated independently of the reactive particles but circulate from the solar receiver to the pyrolysis reactor in which the reactive material is introduced. In the latter concept, the reactants are heated directly by concentrated solar radiation through a transparent window. The reactant can be massive or particulate in form. The reactants are heated only in the focal zone. To achieve high conversions of the particulate feedstock, the reactor, with optimized hydrodynamics for the reactants passing the focal zone, should be chosen in order to control the residence time at high temperatures. In the case of massive feedstocks, one can imagine a cylinder with the same size as the focus of the concentrating system that moves slowly through the focal zone with a velocity corresponding to the reaction time; this concept was demonstrated at the lab scale for volatile oxide reduction, as described in Chambon et al. (2011). The sequential extraction of char should be implemented for biomass pyrolysis. More generally, because of the specificities of the reactions involved in solar pyrolysis, it is likely that the gas-solid reactors that are usually considered in chemical engineering are not the best option. New concepts have to be imagined and future solar pyrolysis reactors will be different from classical reactor designs (Lédé, 1999).

(b) How does one choose the solar reactor material?

In the case of directly heating the feedstock, a window is used for enabling concentrated solar radiation to impinge on the reactants. Quartz windows are transparent to solar radiation and resist high temperatures up to approximately 1200 °C. Borosilicate glass windows are another option that can withstand temperatures up to approximately 600 °C. However, some pyrolysis process that occur at high temperatures produce byproducts (tar and char). In this case, the solar reactor window must be constantly cooled and flooded with inert gases to avoid any contamination or damage from the reacting particles and products. However, this technique has been only partially successful and will need further research for commercialization (Agrafiotis et al., 2014). The insulating and inner materials of the solar reactor must withstand very high temperatures, at least 1200 °C. In addition, they must tolerate large thermal gradients and high heating rates. Moreover, special materials are needed for resisting the thermal stresses caused by concentrated solar radiation. Concerning chemical compatibility, the pyrolysis gases are reducing species; consequently, the inner materials should be inert to high temperature reducing gases.

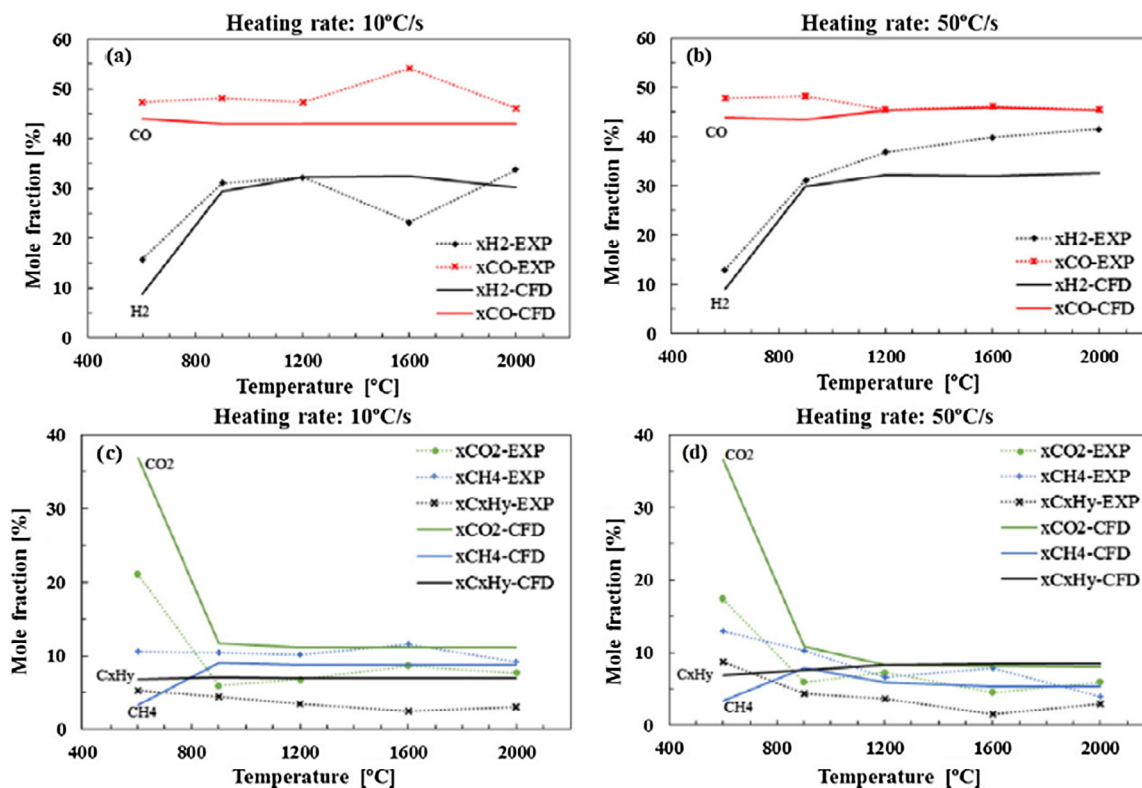


Fig. 18. Comparison of the permanent gas species compositions between the experimental results and CFD predictions. (a) CO and H₂ at 10 °C/s, (b) CO and H₂ at 50 °C/s, (c) CO₂, CH₄ and CxHy (C₂H₂, C₂H₄ and C₂H₆) at 10 °C/s and CO₂, CH₄ and CxHy at 50 °C/s (after Soria et al., 2017).

(c) How can the solar reactor be scaled up?

Scaling up is always a difficult task, even in classical chemical engineering. For solar chemical engineering, additional issues must be considered, such as interfacing the megawatt concentrated solar beam with the reactor (Pitz-Paal et al., 2011), modeling the heat and two-phase flows and coupling heat and mass transfer with the reaction kinetics. Generally, the published pyrolysis kinetic data have been obtained using thermogravimetric analyses (TGA) corresponding to slow heating rates and temperatures limited to approximately 1200 °C. Consequently, these data are not valid for

the fast heating rates and high temperatures as used in solar reactors. The solar pyrolysis kinetics, fluid flows, heat transfer mechanisms, mass transfer and optical properties should be determined carefully for scaling up a solar reactor.

(d) How can the solar reactor be continuously operated?

Solar radiation is intermittent, which causes stability and controlling problems for pyrolysis process. The continuous feeding of feedstock, removing and collecting products are critical problems. Thus, it is necessary to develop a solar reactor concept with a good control system that tolerating transient conditions and working with continuous feeding. From this viewpoint, the indirect heating concept that uses particles as a heat transfer fluid may solve these problems.

Adinberg et al. (2004) studied the fast pyrolysis of biomass in a lab-scale reactor filled with potassium and sodium carbonates. They demonstrated that pyrolysis by direct dispersion of biomass particles in high-temperature (800–900 °C) molten salt can provide high-quality syngas with negligible tar and low char residue. Based on these experimental results, they performed the assessment of a commercial-scale solar reactor (Fig. 19).

(e) How does one reduce the cost?

The capital cost of the installed heliostats is typically 50–60% of the solar thermal chemical processing depreciable capital. If the cost of an installed heliostat could be reduced by 1/2, many solar thermal processes would be economical today (Weimer, 2012). The cost of solar reactor is estimated to represent 10–15% of the solar thermal chemical processing initial capital (Steinfeld and Meier, 2004). The solar reactor efficiency depends on the optical quality of the heliostat field (Pitz-Paal et al., 2011). Thus, reaching

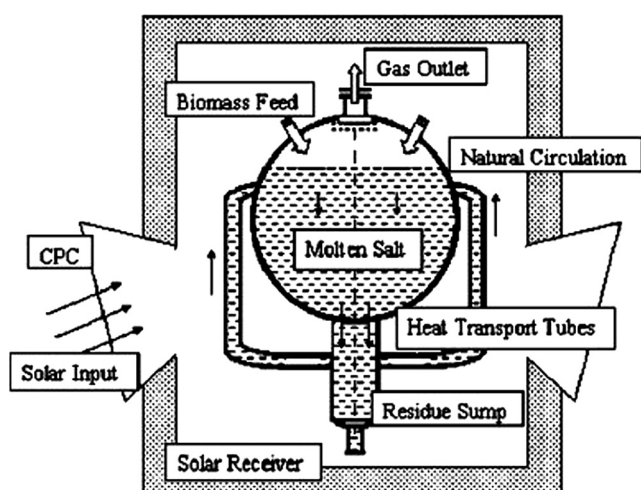


Fig. 19. Schematic of molten salt solar reactor concept (from Adinberg et al. (2004)).

high solar reactor efficiencies and reducing the cost of the heliostats per unit area will have a significant impact on reducing solar pyrolysis costs.

6. Conclusion

In this paper, developments in the field of solar pyrolysis on the basis of its fundamental mechanisms, experimental demonstrations, reactor technology and modeling were reviewed. The majority of the experimental results have been obtained with solar simulators. Antal and his co-workers first performed the biomass solar pyrolysis process with a solar simulator for liquid production because of the quench effects (two temperature reactors). The team of Lédé revealed the presence of short lifetime intermediate liquid compound (ILC) species formed during the flash pyrolysis of cellulose heated with an image furnace. In parallel to these works, large particles were pyrolyzed under radiation from a xenon arc lamp. The heat flux alters the pyrolysis product distribution and the intraparticle temperature evaluation. Parabolic-trough solar collectors and Fresnel lenses have also been used to produce bio-oil through pyrolysis. The latest advances in solar pyrolysis processes have mostly focused on high temperatures and fast heating rates. The aim is to obtain the maximum combustible gas products for heat or power generation. High temperatures ($\geq 1200^\circ\text{C}$) and heating rates ($\geq 50^\circ\text{C/s}$) are interesting for enhancing solar pyrolysis gas (mainly CO and H₂) production from secondary tar reactions. Fuel calorific value upgrading between 21% and 53% (depending on product water content) can be achieved using solar pyrolysis of feedstocks, which enables the storage of solar energy in chemical form. Only particle models have been developed to study the effects of process parameters, such as the radiant heat flux on the solar pyrolysis product distribution. The models demonstrate that secondary tar reactions exist during the solar pyrolysis of large particles.

After reviewing the main advances in the solar pyrolysis process, it can be concluded that these studies have been mainly conducted in the laboratory. After overcoming the technical and economic challenges of solar pyrolysis processes in the future, the solar pyrolysis of carbonaceous feedstocks (coal, biomass and wastes) has the potential to produce high calorific value products with lower CO₂ emissions. In particular, the potential for carbonaceous wastes and polluted biomass solar pyrolysis is very attractive.

Acknowledgments

This work was supported by the French “Investments for the future” program managed by the National Agency for Research, under contract ANR-10-LABX-22-01 (labex SOLSTICE) and contract ANR-10-EQPX-49-SOCRATE (Equipex SOCRATE), and by the FP7 European project STAGE-STE, grant agreement N° 609837.

References

Adinberg, R., Karni, J., Epstein, M., 2004. Solar gasification of biomass: a molten salt pyrolysis study. *J. Sol. Energy Eng.* 126, 850–857.

Agrafiotis, C., VonStorch, H., Roeb, M., Sattler, C., 2014. Solar thermal reforming of methane feedstocks for hydrogen and syngas production—a review. *Renew. Sustain. Energy Rev.* 29, 656–682.

Akhtar, J., Amin, N.S., 2012. A review on operating parameters for optimum liquid. *Renew. Sustain. Energy Rev.* 16, 5101–5109.

Al-Haddad, M., Rendek, E., Corriou, J.P., Mauviel, G., 2010. Biomass fast pyrolysis: experimental analysis and modeling approach. *Energy Fuels* 24, 4689–4692.

Antal, M.J., Hofmann, L., Moreira, J.R., 1980. Bench Scale Radiant Flash Pyrolysis of Biomass. Proceedings of the Specialist's Workshop on Fast Pyrolysis of Biomass; Copper Mountain, CO, Oct 19–22, pp. 175–182.

Antal, M.J., Hofmann, L., Moreira, J., Brown, C.T., Steenblik, R., 1983. Design and operation of a solar-fired biomass flash pyrolysis reactor. *Sol. Energy* 30, 299–312.

Antal, M.J., Mok, W.S.L., Varhegyi, G., Szekely, T., 1990. Review of methods for improving the yield of charcoal from biomass. *Energy Fuels* 4, 221–225.

Authier, O., Lédé, J., 2013. The image furnace for studying thermal reactions involving solids. Application to wood pyrolysis and gasification, and vapours catalytic cracking. *Fuel* 107, 555–569.

Authier, O., Ferrer, M., Mauviel, G., Khalfi, A.-E., Lédé, J., 2009. Wood Fast pyrolysis: comparison of Lagrangian and Eulerian modeling approaches with experimental measurements. *Ind. Eng. Chem. Res.* 48, 4796–4809.

Baumlin, S., Broust, F., Bazer-Bachi, F., Bourdeaux, T., Herbinet, O., Ndiaye, F.T., Ferrer, M., Lédé, J., 2006. Production of hydrogen by lignin fast pyrolysis. *Int. J. Hydrogen Energy* 31, 2179–2192.

Beattie, W.H., Berjoan, R., Coutures, J.-P., 1983. High-temperature solar pyrolysis of coal. *Sol. Energy* 31, 137–143.

Bensaid, S., Centi, G., Garrone, E., Perathoner, S., Saracco, G., 2012. Towards Artificial leaves for solar hydrogen and fuels from carbon dioxide. *ChemSusChem*, 5, 500–521.

Blasi, C.D., 1993. Modeling and simulation of combustion processes of charring and non-charring solid fuels. *Prog. Energy Combust. Sci.* 19, 71–104.

Blasi, C.D., 1996. Heat, momentum and mass transport through a shrinking biomass particle exposed to thermal radiation. *Chem. Eng. Sci.* 51, 1121–1132.

Blasi, C.D., 2008. Modeling chemical and physical processes of wood and biomass pyrolysis. *Prog. Energy Combust. Sci.* 34, 47–90.

Blasi, C.D., Galgano, A., Branca, C., Clemente, M., 2015. Analysis of the interactions between moisture evaporation and exothermic pyrolysis of hazelnut shells. *Energy Fuels* 29, 2514–2526.

Boutin, O., Ferrer, M., Lédé, J., 1998. Radiant flash pyrolysis of cellulose—evidence for the formation of short life time intermediate liquid species. *J. Anal. Appl. Pyrol.* 47, 13–31.

Boutin, O., Ferrer, M., Lédé, J., 2002. Flash pyrolysis of cellulose pellets submitted to a concentrated radiation: experiments and modeling. *Chem. Eng. Sci.* 57, 15–25.

Bridgwater, A.V., Czernik, S., Piskorz, J., 2001. An overview of fast pyrolysis. *Prog. Thermochem. Biomass Convers.* 2, 977–997.

Caubet, S., Corte, P., Fahim, C., Traverse, J.P., 1982. Thermochemical conversion of biomass: gasification by flash pyrolysis study. *Sol. Energy* 29, 565–572.

Chambon, M., Abanades, S., Flamant, G., 2011. Thermal dissociation of compressed ZnO and SnO₂ powders in a moving-front solar thermochemical reactor. *AIChE* 57, 2264–2273.

Chan, W.C., Kelbon, M., Krieger, B.B., 1985. Modelling and experimental verification of physical and chemical processes during pyrolysis of a large biomass particle. *Fuel* 64, 1505–1513.

Chan, W.C., Kelbon, M., Krieger, B.B., 1988. Single-particle biomass pyrolysis: correlations of reaction products with process conditions. *Ind. Eng. Chem. Res.* 27, 2261–2275.

Channiwal, S.A., Parikh, P.P., 2002. A unified correlation for estimating HHV of solid, liquid and gaseous fuels. *Fuel* 81, 1051–1063.

Christodoulou, M., Mauviel, G., Lédé, J., Beaurain, P., Weber, M., Legall, H., Billaud, F., 2013. Novel vertical image furnace for fast pyrolysis studies. *J. Anal. Appl. Pyrol.* 103, 255–260.

Chueh, W.C., Falter, C., Abbott, M., Scipio, D., Furler, P., Haile, S.M., Steinfeld, A., 2010. High-flux solar-driven thermochemical dissociation of CO₂ and H₂O using nonstoichiometric ceria. *Science* 330, 1797–1801.

Czernik, S., Bridgwater, A.V., 2004. Overview of applications of biomass fast pyrolysis oil. *Energy Fuels* 18, 590–598.

Daugaard, D.E., Brown, R.C., 2003. Enthalpy for pyrolysis for several types of biomass. *Energy Fuels* 17, 934–939.

Demibas, A., Arin, G., 2002. An overview of biomass pyrolysis. *Energy Source* 24 (5), 471–482.

Dickerson, T., Soria, J., 2013. Catalytic fast pyrolysis: a review. *Energies* 6, 514–538.

Evans, R.J., Milne, T.A., 1987. Molecular characterization of the pyrolysis of biomass. 1. Fundamentals. *Energy Fuels* 1 (2), 123–137.

Fahmi, R., Bridgwater, A.V., Donnison, I., Yates, N., Jones, J.M., 2008. The effect of lignin and inorganic species in biomass on pyrolysis oil yields, quality and stability. *Fuel* 87, 1230–1240.

Gaur, S., Reed, T.B., 1995. An Atlas of Thermal Data for Biomass and Other Fuels. National Renewable Energy Lab, Golden, CO (United States).

Glaser, P.E., Walker, R.F., 1962. Thermal imaging techniques: proceedings of a conference, Arthur D. Little, Cambridge, MA.

Grønli, M.G., 1996. Thesis of the Norwegian University of Science and Technology, Faculty of Mechanical Engineering.

Grønli, M.G., Melaaen, M.C., 2000. Mathematical model for wood pyrolysis comparison of experimental measurements with model predictions. *Energy Fuels* 14, 791–800.

Haykiri-Acma, H., Yaman, S., Kucukbayrak, S., 2006. Effect of heating rate on the pyrolysis yields of rapeseed. *Renew. Energy* 31, 803–810.

Hofmann, L., Antal, M.J., 1984. Numerical simulations of the performance of solar fired flash pyrolysis reactors. *Sol. Energy* 33, 427–440.

Hopkins, M.W., DeJenga, C., Antal, M.J., 1984. The flash pyrolysis of cellulosic materials using concentrated visible light. *Sol. Energy* 32, 547–551.

Hopkins, M.W., Antal, M.J., Kay, J.G., 1984. Radiant flash pyrolysis of biomass using a xenon flash tube. *J. Appl. Polym. Sci.* 29, 2163–2175.

Hossain, A.K., Davies, P.A., 2013. Pyrolysis liquids and gases as alternative fuels in internal combustion engines - a review. *Renew. Sustain. Energy Rev.* 21, 165–189.

Huber, G.W., Iborra, S., Corma, A., 2006. Synthesis of transportation fuels from biomass: chemistry, catalysts, and engineering. *Chem. Rev.* 106, 4044–4098.

- Hunjan, M.S., Mok, W.S.L., Antal, M.J., 1989. Photolytic formation of free radicals and their effect on hydrocarbon pyrolysis chemistry in a concentrated solar environment. *Ind. Eng. Chem. Res.* 28, 1140–1146.
- IEA, *World Energy Outlook 2014*: IEA.
- Kan, T., Strezov, V., Evans, T., 2016. Lignocellulosic biomass pyrolysis: a review of product properties and effects of pyrolysis parameters. *Renew. Sustain. Energy Rev.* 57, 1126–1140.
- Karayildirim, T., Yanik, J., Yuksel, M., Bockhorn, H., 2006. Characterisation of products from pyrolysis of waste sludges. *Fuel* 85, 1498–1508.
- Kenarsari, S.D., Zheng, Y., 2014. Fast pyrolysis of biomass pellets using concentrated solar radiation: a numerical study. *J. Sol. Energy Eng.* 136, 041004.
- Kodama, T., 2003. High-temperature solar chemistry for converting solar heat to chemical fuels. *Prog. Energy Combust. Sci.* 29, 567–597.
- Lédé, J., 1999. Solar thermochemical conversion of biomass. *Sol. Energy* 65, 3–13.
- Lédé, J., Li, H.Z., Villermaux, J., 1987. Fusion-like behavior of wood pyrolysis. *J. Anal. Appl. Pyrol.* 10, 291–308.
- Lédé, J., Blanchard, F., Boutin, O., 2002. Radiant flash pyrolysis of cellulose pellets: precursors and mechanisms involved in transient and steady state conditions. *Fuel* 81, 1269–1279.
- Li, R., Zeng, K., Soria, J., Mazza, G., Gauthier, D., Rodriguez, R., Flamant, G., 2016. Product distribution from solar pyrolysis of agricultural and forestry biomass residues. *Renew. Energy* 89, 27–35.
- Liang, Y.G., Cheng, B., Si, Y.B., Cao, D.J., Jiang, H.Y., Han, G.M., Liu, X.H., 2014. Thermal decomposition kinetics and characteristics of *Spartina alterniflora* via thermogravimetric analysis. *Renew. Energy* 68, 111–117.
- Liu, C.J., Wang, H.M., AM, K., Sun, J.M., Wang, Y., 2014. Catalytic fast pyrolysis of lignocellulosic biomass. *Chem. Soc. Rev.* 43, 7594–7623.
- Mohan, D., Pittman, C.U., Steele, P.H., 2006. Pyrolysis of wood/biomass for bio-oil: a critical review. *Energy Fuels* 20, 848–889.
- Morales, S., Miranda, R., Bustos, D., Cazares, T., Tran, H., 2014. Solar biomass pyrolysis for the production of bio-fuels and chemical commodities. *J. Anal. Appl. Pyrol.* 109, 65–78.
- Mullen, C.A., Boateng, A.A., Goldberg, N.M., Lima, I.M., Laird, D.A., Hicks, K.B., 2010. Bio-oil and bio-char production from corn cobs and stover by fast pyrolysis. *Biomass Bioenergy* 34, 67–74.
- Neves, D., Thunman, H., Matos, A., Tarelho, L., Gómez-Barea, A., 2011. Characterization and prediction of biomass pyrolysis products. *Prog. Energy Combust. Sci.* 37, 611–630.
- Neves, D., Thunman, H., Matos, A., Tarelho, L., Gómez-Barea, A., 2011. Characterization and prediction of biomass pyrolysis products. *Prog. Energy Combust. Sci.* 37, 611–630.
- Nzihou, A., Flamant, G., Stanmore, B., 2012. Synthetic fuels from biomass using concentrated solar energy - a review. *Energy* 42, 121–131.
- Piatkowski, N., Wieckert, C., Steinfeld, A., 2009. Experimental investigation of a packed-bed solar reactor for the steam gasification of carbonaceous feedstocks. *Fuel Process. Technol.* 90, 360–366.
- Piatkowski, N., Wieckert, C., Weimer, A., Steinfeld, A., 2011. Solar-driven gasification of carbonaceous feedstock—a review. *Energy Environ. Sci.* 4, 73–82.
- Pitz-Paal, R., Bayer Botero, N., Steinfeld, A., 2011. Heliostats field layout optimization for high-temperature solar thermochemical processing. *Sol. Energy* 85, 334–343.
- Pozzobon, V., Salvador, S., Bézian, J.J., El-Hafi, M., Le Maout, Y., Flamant, G., 2014. Radiative pyrolysis of wet wood under intermediate heat flux: experiments and modelling. *Fuel Process. Technol.* 128, 319–330.
- Pütün, A.E., 2002. Biomass to bio-oil via fast pyrolysis of cotton straw and stalk. *Energy Source* 24, 275–285.
- REN21, *Global Status Report 2014*.
- Romero, M., Steinfeld, A., 2012. Concentrating solar thermal power and thermochemical fuels. *Energy Environ. Sci.* 5, 9234–9245.
- Soria, J., Zeng, K., Asensio, D., Gauthier, D., Flamant, G., Mazza, G., 2017. Comprehensive CFD modelling of solar fast pyrolysis of beech wood pellets. *Fuel Process. Technol.* 158, 226–237.
- Steinfeld, A., Meier, A., 2004. Solar fuels and materials. *Encyclopedia Energy* 5, 623–637.
- Tabatabaie-Raissi, A., Antal, M.J., 1986. Design and operation of a 30 KWe/2 KWth downward facing beam ARC image furnace. *Sol. Energy* 36, 419–429.
- Tabatabaie-Raissi, A., Mok, W.S.L., Antal, M.J., 1989. Cellulose pyrolysis kinetics in a simulated solar environment. *Ind. Eng. Chem. Res.* 28, 856–865.
- Vamvuka, D., Sfakiotakis, S., 2011. Effects of heating rate and water leaching of perennial energy crops on pyrolysis characteristics and kinetics. *Renew. Energy* 36, 2433–2439.
- Van de Velden, M., Baeyens, J., Brems, A., Janssens, B., Raf, D., 2010. Fundamentals, kinetics and endothermicity of the biomass pyrolysis reaction. *Renew. Energy* 35, 232–242.
- Weimer, A., 2012. Solar thermal chemical processing challenges and commercial path forward. *Curr. Opin. Chem. Eng.* 1, 211–217.
- Wieckert, C., Obrist, A., von Zedtwitz, P., Maag, G., Steinfeld, A., 2013. Syngas production by thermochemical gasification of carbonaceous waste materials in a 150 kWth packed-bed solar reactor. *Energy Fuel* 27, 4770–4776.
- Yadav, D., Banerjee, R., 2016. A review of solar thermochemical processes. *Renew. Sustain. Energy Rev.* 54, 497–532.
- Zeaiter, J., Ahmad, M.N., Rooney, D., Samneh, B., Shamma, E., 2015. Design of an automated solar concentrator for the pyrolysis of scrap rubber. *Energy Convers. Manage.* 101, 118–125.
- Zeng, K., Gauthier, D., Flamant, G., 2014. High temperature flash pyrolysis of wood in a lab-scale solar reactor. In: *Proceedings of ASME 2014 8th International Conference on Energy Sustainability*. Boston, USA (June 30–July 2).
- Zeng, K., Flamant, G., Gauthier, D., Guillot, E., 2015. Solar pyrolysis of wood in a lab-scale solar reactor: influence of temperature and sweep gas flow rate on products distribution. *Energy Proc.* 69, 1849–1858.
- Zeng, K., Minh, D.P., Gauthier, D., Weiss-Hortala, E., Nzihou, A., Flamant, G., 2015a. The effect of temperature and heating rate on char properties obtained from solar pyrolysis of beech wood. *Biores. Technol.* 182, 114–119.
- Zeng, K., Gauthier, D., Li, R., Flamant, G., 2015b. Solar pyrolysis of beech wood: effects of pyrolysis parameters on the product distribution and gas product composition. *Energy* 93, 1648–1657.
- Zeng, K., Gauthier, D., Lu, J., Flamant, G., 2015c. Parametric study and process optimization for solar pyrolysis of beech wood. *Energy Convers. Manage.* 106, 987–998.
- Zeng, K., Soria, J., Gauthier, D., Mazza, G., Flamant, G., 2016. Modeling of beech wood pellet pyrolysis under concentrated solar radiation. *Renew. Energy* 99, 721–729.
- Zeng, K., Gauthier, D., Minh, D.P., Weiss-Hortala, E., Nzihou, A., Flamant, G., 2017a. Characterization of solar fuels obtained from beech wood solar pyrolysis. *Fuel* 188, 285–293.
- Zeng, K., Gauthier, D., Li, R., Flamant, G., Gilles, 2017b. Combined effects of initial water content and heating parameters on solar pyrolysis of beech wood. *Energy* 125, 552–561.